Topological spin Meissner effect in spinor exciton-polariton condensate: Constant amplitude solutions, half-vortices, and symmetry breaking

Dmitry R. Gulevich,[1,2,*] Dmitry V. Skryabin,[1,2] Alexander P. Alodjants,[1] and Ivan A. Shelykh[1,3,4]
[1]*ITMO University, St. Petersburg 197101, Russia*
[2]*Department of Physics, University of Bath, Bath BA2 7AY, United Kingdom*
[3]*Science Institute, University of Iceland, Dunhagi 3, IS-107, Reykjavik, Iceland*
[4]*Division of Physics and Applied Physics, Nanyang Technological University 637371, Singapore*
(Received 10 May 2016; revised manuscript received 11 August 2016; published 2 September 2016)

We generalize the spin Meissner effect for an exciton-polariton condensate confined in annular geometries to the case of nontrivial topology of the condensate wave function. In contrast to the conventional spin Meissner state, topological spin Meissner states can in principle be observed at arbitrary high magnetic fields not limited by the critical magnetic field value for the condensate in a simply connected geometry. One special example of the topological Meissner states are half-vortices. We show that in the absence of magnetic field, half-vortices in a ring exist in a form of a superposition of elementary half-vortex states, which resolves recent experimental results where such puzzling superposition was observed. Furthermore, we show that if a pure half-vortex state is to be observed, a nonzero magnetic field of a specific magnitude needs to be applied. Studying exciton polaritons in a ring in the presence of TE-TM splitting, we observe spin Meissner states that break the rotational symmetry of the system by developing inhomogeneous density distributions. We classify various states arising in the presence of nonzero TE-TM splitting based on what states they can be continued from by increasing the TE-TM splitting parameter from zero. With further increasing TE-TM splitting, states with broken symmetry may transform into stable half-dark solitons and therefore may serve as a useful tool to generate various nontrivial states of a spinor condensate.

DOI: 10.1103/PhysRevB.94.115407

I. INTRODUCTION

Development of nanotechnology achieved during the last decade allowed the design of semiconductor microcavities possessing extremely high Q factors (more than 10 000). This opened new opportunities in creation and investigation of fundamental properties of Bose-Einstein condensates (BEC) of exciton polaritons—hybrid light-matter quasiparticles emerging in the regime of strong coupling [1]. Although, strictly speaking, the thermodynamic equilibrium of exciton polaritons is rarely achieved, they exhibit properties inherent to weakly interacting quantum Bose-gases. Among them is superfluidity [2,3], formation of quantized vortices [4,5] and solitons [6], Josephson oscillations and macroscopic self-trapping [7], the spin-Hall effect [8] and others. The peculiarity of the spin structure of polaritons combined with strong polariton-polariton interactions and large coherence lengths makes possible the generation of coherent bosonic spin currents [9]. This opens a new research field of light-mediated spin effects and paves the way for their implementation in optoelectronics, e.g., for the creation of all-optical integrated circuits [10,11].

Polariton systems possess several advantages with respect to systems based on cold atoms. First, the extremely small mass of polaritons (about 10^{-5} of the mass of free electrons) makes critical temperatures of the observation of quantum collective effects surprisingly high (from a few Kelvin for GaAs-based structures to room temperature for GaN structures [12]). Besides, polariton condensates allow reasonably simple manipulation by application of external electric and magnetic fields [13,14]. This plays essential role in the study of the fundamental properties of exciton-polariton condensates. In the general case, magnetic field affects the exciton-polariton emission energy, linewidth, and intensity due to the exciton energy shift caused by Zeeman splitting in circular polarizations, the modification of the exciton-photon coupling strength [15], and the modification of scattering process with acoustic phonons [16]. The strong spin anisotropy of polariton-polariton interactions, however, makes those dependencies in the nonlinear regime highly nontrivial. In particular, in Ref. [17], it was shown that below some critical value B_c of the magnetic field, depending on the polariton concentration, the so-called full paramagnetic screening (also known as spin Meissner effect) occurs. Its signature is independence of the photoluminescence energy on the magnetic field. The latter, however, affects the polarization of the emission. Its ellipticity gradually changes until the value B_c is reached. At this point, emission becomes fully circular polarized and Zeeman splitting re-establishes. The main efforts of recent experimental studies of exciton-polariton condensates in a magnetic field have been successfully directed towards confirmation of these seminal peculiarities, cf. Refs. [16,18–21].

The interplay between polarization splitting and anisotropic polariton-polariton interactions becomes more tricky in anisotropic cavities when additional energy splittings in linear polarizations (TE-TM splittings) are present in addition to the Zeeman splitting [22]. The situation becomes even more interesting when polaritons are confined in nonsimply connected regions, e.g., inside a ring resonator. In this case, the direction of the effective magnetic field provided by TE-TM splitting becomes position-dependent, which combined together with a magnetic-field-induced Zeeman splitting leads to the appearance of the geometric Berry phase responsible for the generation of a synthetic U(1) gauge field for polaritons and possibility for the observation of an optical

*d.r.gulevich@lmc.ifmo.ru

analog of the Aharonov-Bohm effect [23]. It should be noted that exciton-polariton spinor BECs in a ring geometry have been experimentally demonstrated by several groups [11,18–20,24,25]. However, the polarization properties of the interacting spinor polaritons in the rings were not subject of theoretical investigation up to now to the best of our knowledge. On the other hand, the presence of an artificial U(1) gauge potential can lead to the onset of a persistent current in the system, i.e., its ground state can be a vortex-type solution. The investigation of the analogs of the spin Meissner effect for such states with a quantized angular momentum is a fundamentally interesting problem which can in principle lead to applications such as polariton flux qubits.

Spinor vortex-type solutions in 2D systems were analyzed in Ref. [26]. It was shown that besides normal vortices for which both circular polarization components have the same nonzero quantized angular momentum, half-vortex solutions for which one of the circular polarizations is not rotating. Half-vortices had been detected experimentally [5], but their stability in 2D condensate in the presence of TE-TM splitting remained a topic of a debate [27–29]. The current view is that small TE-TM splitting does not destroy half-vortices leading only to their warping [30]. However, large TE- TM splittings can make in principle half-vortex solutions unstable. This situation may become relevant when the polaritons are confined in the ring, where relevant splittings can reach the values of 1–2 meV for ring thicknesses of about one micrometer [31]. Recent experimental work on half-vortices in a ring geometry [24] demonstrated that polarization patterns and density profiles could not be explained by the existing theory, which led the authors to a conclusion that their experimental configuration corresponds to some spurious superposition of certain "elementary" half-vortex states.

The aim of this paper is to provide a theory of interacting polariton ring condensate, introduce the concept of the topological spin Meissner effect, and describe the rich variety of the states of the condensate both in the presence and absence of the TE-TM splitting. In particular, we provide a detailed analysis of the half-vortex states in the ring and show that the superpositions of elementary half-vortex states reported experimentally in Ref. [24] appear naturally in the developed theory.

The paper is organized as follows. In Sec. II, we present the model of exciton-polariton condensate in a ring and introduce various types of emerging solutions. In Sec. III, we introduce the topological spin Meissner effect in the case when the TE-TM splitting is absent. In Secs. IV and V, we extend the concepts and solutions obtained in the previous section to the general case of finite TE-TM splitting. More specifically, Sec. IV deals with topological spin Meissner states in the form of constant-amplitude solutions, and in Sec. V, we study states that spontaneously break the rotational symmetry of the system due to the presence of TE-TM splitting. Section VI contains a discussion of the experimental relevance of our parameters.

II. MODEL AND CLASSIFICATION OF SOLUTIONS

Interacting polaritons trapped in a quasi-one-dimensional ring resonator can be described by the following system of dimensionless Gross-Pitaevskii equations (see Appendix A):

$$\begin{aligned} i\dot{\psi}_+ &= -\partial_x^2\psi_+ + (|\psi_+|^2 + \alpha|\psi_-|^2)\psi_+ \\ &\quad + \Omega\psi_+ + \kappa e^{-2ix}\psi_-, \\ i\dot{\psi}_- &= -\partial_x^2\psi_- + (|\psi_-|^2 + \alpha|\psi_+|^2)\psi_- \\ &\quad - \Omega\psi_- + \kappa e^{2ix}\psi_+. \end{aligned} \tag{1}$$

Here, $\psi_\pm$ are the components of the exciton-polariton spinor wave function $\boldsymbol{\psi} \equiv \{\psi_+, \psi_-\}$ in the basis of circular polarizations satisfying $\psi_\pm(t,x) = \psi_\pm(t, x+2\pi)$, x is the azimuthal angle, parameter $\alpha < 0$ characterizes the attractive interaction of the cross-polarized polaritons, Ω is half of Zeeman splitting of a free polariton state (which we will refer to as just "magnetic field"), and κ is half of the momentum-independent TE-TM energy splitting. Parameters Ω and κ are dimensionless and scale in units of $\hbar^2/(2m^*R^2)$, where R is the ring radius and m^* is the exciton-polariton effective mass. We use the dimensionless particles density per unit length, $\rho \equiv \frac{1}{2\pi}\int_0^{2\pi}(|\psi_+|^2 + |\psi_-|^2)dx$, as a parameter controlling the strength of the polariton-polariton interactions.

To study the stationary states of the system (1), we use the substitution

$$\psi_\pm(t,x) = \psi_\pm(x)e^{-i\mu t}. \tag{2}$$

We treat μ as an unknown variable corresponding to the energy blue shift of a photoluminescence line of the condensate in a steady state [32], found for a given ρ. It is also identical to the chemical potential parameter used in the literature on the Gross-Pitaevskii model and Bose-Einstein condensation. When time-dependent problems are treated, μ gives the frequency of the rotating frame in which the dynamics of physical quantities is captured.

The system of equations (1) inherits properties of the nonlinear Schrödinger equation. Similar to the nonlinear Schrödinger equation [33], an important class of stationary solutions of Eqs. (1) is constant-amplitude solutions, which correspond to polarization vortices with the homogeneous density distributions along the ring. Those can be sought in the form

$$\psi_\pm(x) = \chi_\pm e^{im_\pm x}, \quad \text{for} \quad \kappa = 0 \tag{3}$$

and

$$\psi_\pm(x) = \chi_\pm e^{i(n\mp 1)x}, \quad \text{for} \quad \kappa \neq 0. \tag{4}$$

Here, $\chi_\pm$ are x-independent amplitudes. Therefore in the presence of the TE-TM splitting vortex the winding numbers in the two components of the spinor must differ by 2, while these winding numbers $m_\pm$ are arbitrary integers for $\kappa = 0$. In the limit of noninteracting polaritons, μ gives the energy spectrum, and the existence of solutions (4) and (3) requires

$$\mu = \mu_\pm^{(0)}, \quad \mu_\pm^{(0)} = m_\pm^2 \pm \Omega \tag{5}$$

and

$$\mu = \mu_\pm, \quad \mu_\pm = 1 + n^2 \pm \sqrt{(2n-\Omega)^2 + \kappa^2}, \tag{6}$$

respectively. It is clear that the vortex energies in the no-interaction limit vary linearly with the applied magnetic field Ω for $\kappa = 0$. While for $\kappa \neq 0$, one deals with the typical

anticrossing behavior in the proximity of the points $\Omega = 2n$ (see detailed discussion and figure in Sec. IV).

When nonlinear effects are included, the energies acquire the corresponding nonlinear shifts proportional to ρ, but not only this. The spin anisotropy of nonlinear interaction $\alpha \neq 1$ makes it possible for the mixed ($\chi_+ \neq 0, \chi_- \neq 0$) vortex states to loose the dependence of their energies on the applied magnetic field. Such behavior of exciton-polariton condensate in thermodynamic equilibrium is known as spin Meissner effect (for an introduction to the spin Meissner effect see Sec. I and original Refs. [17,18,22]). However, in contrast to the previously studied spin Meissner effect, the properties of such vortex states and their domain of existence are defined by the vortex winding numbers. To highlight the dependence on the winding numbers, we term the vortex states whose energies either exactly or approximately lose dependence on the magnetic field—*topological spin Meissner states* (TSM states). As it will be shown below, TSM states are a ubiquitous feature of our model. Note, that vortices with $m_+ = \pm 1$, $m_- = 0$, and $m_+ = 0$, $m_- = \pm 1$ are so-called half-vortices in the terminology used in Refs. [5,26–30]. We will show that half-vortices also exhibit the topological spin Meissner effect.

We study nonlinear solutions for $\kappa = 0$ in Sec. III. Importantly, solutions (3) with $m_- - m_+ \neq 2$, do not disappear as we introduce $\kappa \neq 0$, they simply develop inhomogeneous density profiles and thus are associated with breaking the rotational symmetry. We study the $\kappa \neq 0$ case in details in Sec. IV. Note that the system of Eq. (1) even with $\kappa = 0$ has various solitonlike solutions with inhomogeneous density profiles, see, e.g., Ref. [33]. These solitons can continue to exist for nonzero κ as well. In order to limit the scope of the present work, we leave these type of inhomogeneous solutions for future studies.

III. TOPOLOGICAL SPIN MEISSNER EFFECT: ZERO TE-TM SPLITTING

A. Stationary solutions

We first focus on the case when the TE-TM splitting is absent, $\kappa = 0$. Substituting Eq. (3) into (1), we have

$$\begin{aligned}[-\mu + m_+^2 + \chi_+^2 + \alpha\chi_-^2 + \Omega]\chi_+ = 0,\\ [-\mu + m_-^2 + \chi_-^2 + \alpha\chi_+^2 - \Omega]\chi_- = 0.\end{aligned} \tag{7}$$

Because the phases of $\psi_\pm$ are arbitrary, in this section, we will assume $\chi_-, \chi_+ \geqslant 0$ without loosing the generality, however, the relative phase of the amplitudes will play an important role when we will be dealing with the case of nonzero TE-TM splitting in the next section. One obvious class of solutions of Eq. (7) comes by setting either χ_+ or χ_- to zero: this gives two solutions with amplitudes $(\chi_+, \chi_-) = (\sqrt{\rho}, 0)$ and $(\chi_+, \chi_-) = (0, \sqrt{\rho})$ and chemical potentials

$$\mu_+^{(0)} = m_+^2 + \rho + \Omega \tag{8}$$

and

$$\mu_-^{(0)} = m_-^2 + \rho - \Omega, \tag{9}$$

respectively. Energies of these solutions either increase or decrease with Ω, depending on whether the polariton spin is parallel or antiparallel to the applied magnetic field.

The other distinct class of solutions corresponds to the case when both components have nonzero densities, $\chi_+, \chi_- \neq 0$. Equating the expressions in square brackets in (7) and using the normalization $\chi_+^2 + \chi_-^2 = \rho$, we find

$$\chi_+^2 = \frac{\rho - z}{2}, \quad \chi_-^2 = \frac{\rho + z}{2}, \tag{10}$$

where

$$z = \frac{2(\Omega - \Omega_c)}{(1 - \alpha)} \tag{11}$$

and

$$\Omega_c = \tfrac{1}{2}(m_-^2 - m_+^2) = 0, \pm\tfrac{1}{2}, \pm\tfrac{3}{2}, \pm 2, \ldots. \tag{12}$$

Solutions (10) depend on the magnetic field via parameter $z = \chi_-^2 - \chi_+^2$ subjected to the condition $|z| < \rho$. Therefore solutions exist only in a limited interval of Ω given by

$$|\Omega - \Omega_c| < \rho\,\frac{(1 - \alpha)}{2}, \tag{13}$$

and centered around Ω_c. Note that $\Omega = \Omega_c$ ($z = 0$) for different m_+, m_- are degeneracy points at which energies (8) and (9) of the circularly polarized solutions coincide.

Substituting (10) into (7), we find a chemical potential for the mixed polarization states (10):

$$\mu^{(0)} = \tfrac{1}{2}[m_+^2 + m_-^2 + \rho(1 + \alpha)]. \tag{14}$$

Thus the chemical potential $\mu = \mu^{(0)}$ in this case does not depend on the magnetic field and according to the terminology introduced in Sec. II, these are the topological spin Meissner (TSM) states. Equations (10), (13), and (14) are a generalization of the conventional spin Meissner effect to the case when the spinor components possess a nontrivial phase winding and therefore can be called a *topological* spin Meissner effect (TSM effect) [34]. The conventional spin Meissner effect [17,18,22] arises when spin-dependent polariton-polariton interactions compensate the Zeeman splitting. Such compensation is possible until the fully circularly polarized state is reached. In the TSM effect, the Zeeman splitting is compensated by the combined action of both polariton-polariton interactions and the circulation of the exciton-polariton condensate described by the winding numbers m_+, m_-. Note that for TSM states to exist, the offset of the magnetic field Ω from its critical values Ω_c should be small enough, see Eq. (13). The graphs of μ versus Ω and μ versus ρ for the families of solutions (8), (9), and (10) are shown in Figs. 1(a) and 1(b), respectively. The linear spectrum (5) is recovered in the limit $\rho \to 0$, see Fig. 1(b).

At a fixed magnetic field, the condition (13) defines the minimal value of the nonlinearity parameter ρ, which is needed to observe a given TSM state. Equations (12) and (13) at $\Omega = 0$ give the existence criterion for a TSM state with the winding numbers m_+ and m_-,

$$\rho > \rho_{\min}(m_+, m_-) \equiv \frac{|m_-^2 - m_+^2|}{1 - \alpha}. \tag{15}$$

Therefore more and more TSM states arise as nonlinearity is gradually increased from zero. The appearance of TSM states with increasing nonlinearity is seen on the $\mu(\rho)$ plot on Fig. 1(b) and $\mu(\Omega)$ plot on Fig. 2. As seen from Fig. 1(b),

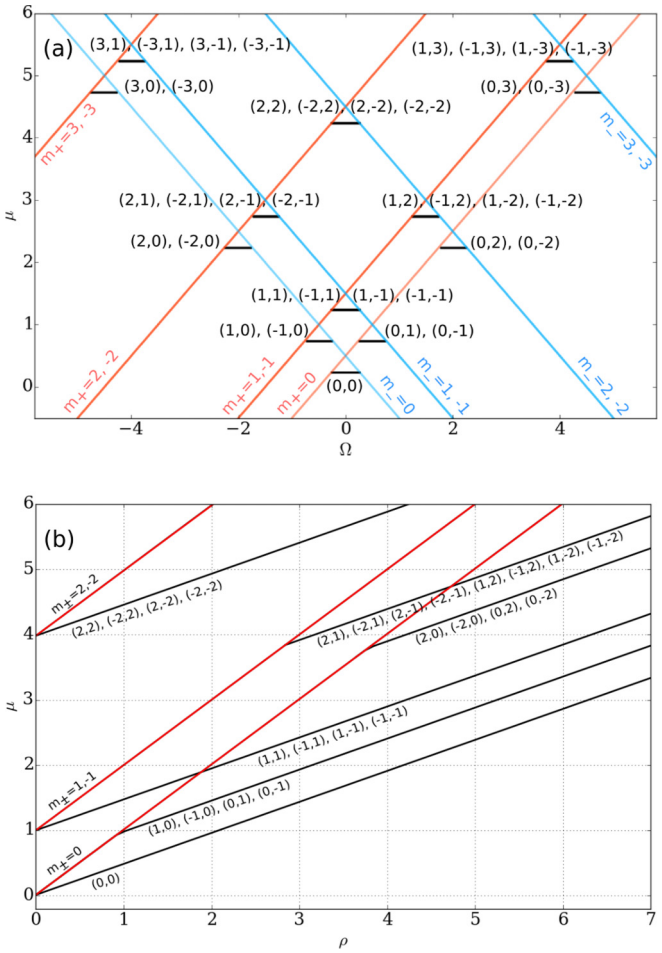

FIG. 1. Families of constant-amplitude solutions (3) in zero TE-TM splitting ($\kappa = 0$) on the diagrams μ vs Ω at fixed $\rho = 0.5$ (a) and μ vs ρ at fixed $\Omega = 0$. Red and blue solid lines are pure circular polarization vortices characterized by winding numbers $m_\pm$ and the chemical potential is given by Eqs. (8) and (9). Black lines are topological spin Meissner (TSM) states specified by a pair of winding numbers (m_+,m_-). Each TSM state appears from the interaction of circular polarization vortices, and if the nonlinearity is increased from zero, they arise from the corresponding intersections of the red and blue lines in (a). (b) shows how TSM states appear on the diagram μ vs ρ when the nonlinearity parameter is increased continuously from $\rho = 0$ (linear case) to 7 in zero magnetic field $\Omega = 0$. In both cases, $\alpha = -0.05$.

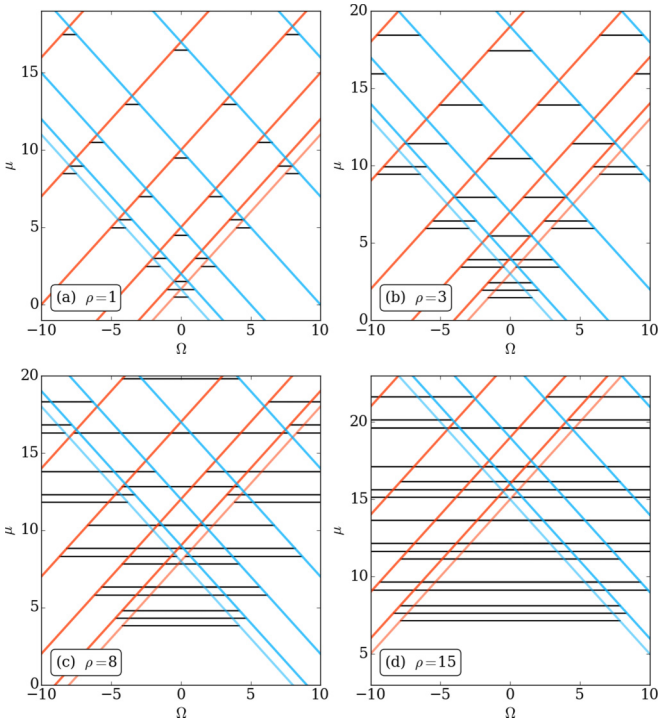

FIG. 2. Constant-amplitude solutions (3) in zero TE-TM splitting ($\kappa = 0$) on the diagrams μ vs Ω at different values of the nonlinearity parameter $\rho = 1$ (a), 3 (b), 8 (c), and 15 (d). Topological spin Meissner (TSM) states are marked by black lines resting on the corresponding red and blue diagonal lines corresponding to the pure circular polarization vortices. The intervals of magnetic field where a given TSM state exists grow with increasing nonlinearity ρ. More details are provided in Fig. 1 where the specific TSM states are marked by their winding numbers. In all cases, $\alpha = -0.05$.

TSM states with $|m_+| = |m_-|$ start off straight from the linear spectrum ($\rho = 0$), while those with $|m_+| \neq |m_-|$ require a finite value of nonlinearity given by (15). In presence of large nonlinearity, TSM states are the lowest energy states of the system and arrange into a system of energy levels as shown in Fig. 2.

An illustrative example of TSM effect is the behavior of half-vortices in the presence of a magnetic field. Similar to half-vortices in a 2D system [26,27], *half-vortices in a ring* have zero phase winding number of one component and a simple vortex in the other component. These are four distinct states: (1,0), (−1,0), (0,1), and (0,−1). These are essentially nonlinear states which cease to exist in the linear limit, see Fig. 1(b). In zero magnetic field, half-vortices may only be observed for the nonlinearities stronger than the critical value $\rho > 1/(1-\alpha)$ given by the formula (15). On the other hand, if the magnetic field is tuned to $\Omega = \Omega_c = \pm 1/2$, even a very small nonlinearity would be enough to create a half-vortex.

In order to compare our findings with existing experimental studies of half-vortices in rings [24], we change to the basis of linear polarization. At $z = 0$, the constant-amplitude solution (3) with amplitudes defined by (10) takes the form

$$\psi_{\rm lin}(z=0) = \sqrt{\rho}\,\exp\left(i\frac{m_+ + m_-}{2}x\right)\begin{pmatrix}\cos\frac{\Delta m}{2}x\\ \sin\frac{\Delta m}{2}x\end{pmatrix}, \quad (16)$$

where the two components of the spinor in the basis of linear polarization are $\psi_{\rm lin,1} = (\psi_+ + i\psi_-)/\sqrt{2}$ and $\psi_{\rm lin,2} = (\psi_+ - i\psi_-)/\sqrt{2}$. Note that the implicit choice of the relative phase of the spinor components $\chi_+ = \chi_-$ made here is arbitrary: half-vortex states with different relative phase of χ_+ and χ_- are connected by a simple shift of coordinate as will be shown in Sec. V. For Ω away from Ω_c, the expression for a half-vortex in linear polarization becomes more involved. A simple expression may be obtained assuming $z/\rho \ll 1$,

$$\psi_{\rm lin} \approx \psi_{\rm lin}(z=0) + i\frac{z}{\rho}\begin{pmatrix}\sin\frac{\Delta m}{2}x\\ -\cos\frac{\Delta m}{2}x\end{pmatrix}. \quad (17)$$

The formula (17) can explain the experimental result [24] where a superposition of half-vortex states was observed. According to Ref. [24], the ansatz in the form of superposition of states of the type (16) was used to fit the experimental data. This puzzling result could not be explained by the existing theory but created an uncertainty of why half-vortices prefer a superposition in favor of a pure state (16). Assuming the experiments were done in zero magnetic field we find that $|z| = 1/(1-\alpha) \neq 0$. Therefore formula (17) makes it clear that a pure half-vortex state in the form (16) can not be observed in zero magnetic field. Furthermore, if a pure half-vortex state (16) is to be observed, a nonzero magnetic field with magnitude equal exactly to $|\Omega| = 1/2$ should be applied. As far as we know, this has not been done in the existing experimental studies of exciton-polariton states in a ring.

B. Stability of spin Meissner states

To analyze stability, we consider small time-dependent perturbations $\varepsilon_\pm(x,t)$ around vortices:

$$\psi_\pm(x,t) = [\chi_\pm + \varepsilon_\pm(x,t)]e^{im_\pm x}. \tag{18}$$

Substituting (18) into (1) at $\kappa = 0$, we get a system of linear equations for $\varepsilon_\pm(x,t)$,

$$\begin{aligned} i\dot{\varepsilon} = &-\varepsilon_\pm'' - 2im_\pm\varepsilon_\pm' + \chi_\pm^2(\varepsilon_\pm + \varepsilon_\pm^*) \\ &+ \alpha\chi_\pm\chi_\mp(\varepsilon_\mp + \varepsilon_\mp^*) = 0 \end{aligned} \tag{19}$$

Expanding $\varepsilon_\pm(x,t)$ into Fourier series in x, see, e.g., Ref. [35],

$$\varepsilon_\pm(x,t) = \sum_{l=0}^{\infty} U_{\pm,l}(t)e^{ilx} + V_{\pm,l}^*(t)e^{-ilx}, \tag{20}$$

we get a system of equations on $\mathbf{W}_l(t) = (U_{+,l}, V_{+,l}, U_{-,l}, V_{-,l})$, decoupled for different integer l,

$$i\dot{\mathbf{W}}_l = \hat{\eta}\hat{\mathcal{H}}_l\mathbf{W}_l, \tag{21}$$

where

$$\hat{\eta} = \begin{pmatrix} 1 & 0 & 0 & 0 \\ 0 & -1 & 0 & 0 \\ 0 & 0 & 1 & 0 \\ 0 & 0 & 0 & -1 \end{pmatrix} \tag{22}$$

and

$$\hat{\mathcal{H}}_l = \begin{pmatrix} d_+ & \chi_+^2 & \alpha\chi_+\chi_- & \alpha\chi_+\chi_- \\ \chi_+^2 & \tilde{d}_+ & \alpha\chi_+\chi_- & \alpha\chi_+\chi_- \\ \alpha\chi_+\chi_- & \alpha\chi_+\chi_- & d_- & \chi_-^2 \\ \alpha\chi_+\chi_- & \alpha\chi_+\chi_- & \chi_-^2 & \tilde{d}_- \end{pmatrix}, \tag{23}$$

where $d_\pm \equiv l^2 + 2lm_\pm + \chi_\pm^2, \tilde{d}_\pm \equiv l^2 - 2lm_\pm + \chi_\pm^2$. Assuming $\mathbf{W}_l = \mathbf{w}_l e^{-i\lambda t}$, $\mathbf{w}_l \equiv (u_{+,l}, v_{+,l}, u_{-,l}, v_{-,l})$, we get an eigenvalue problem:

$$\hat{\eta}\hat{\mathcal{H}}_l\mathbf{w}_l = \lambda\mathbf{w}_l. \tag{24}$$

The solution is spectrally unstable if there is at least one eigenvalue with positive imaginary part $\mathrm{Im}\,\lambda > 0$. Because of equality $\mathrm{Tr}[(\hat{\eta}\hat{\mathcal{H}}_l)^\dagger] = \mathrm{Tr}[\hat{\eta}\hat{\mathcal{H}}_l]$, the eigenvalues of the matrix $\hat{\eta}\hat{\mathcal{H}}_l$ come in complex conjugated pairs.

In the special case $\Omega = \Omega_c$, the eigenvalue problem [(24) and (23)] allows simple analytical solution. For $\Omega = \Omega_c$, we have, according to (10), $\chi_+ = \chi_- = \sqrt{\rho/2}$. Substituting into (24) and (23) and solving the eigenvalue problem, we get four eigenvalues:

$$\begin{aligned} \lambda = l\Big(&m_+ + m_- \\ &\pm\sqrt{\Delta m^2 + l^2 + \rho \pm \sqrt{4\Delta m^2(l^2+\rho) + \alpha^2\rho^2}}\Big), \end{aligned} \tag{25}$$

where

$$\Delta m \equiv m_- - m_+. \tag{26}$$

From (25), the unstable regions can be easily found,

$$|l^2 + \rho - \Delta m^2| < \alpha\rho. \tag{27}$$

It is straightforward to see from (27) that there is no instability in the case $\alpha = 0$ when interaction between the circular components is absent. However, for finite α, we have an unstable region in ρ extending up to $\Delta\rho \approx |\alpha|\rho_c$ either side from $\rho_c = \Delta m^2 - l^2$.

We analyze the stability for arbitrary values of Ω by using the perturbation theory in parameter α. We take into account the dependence of χ_+ and χ_- on α exactly using their expressions (10), while we treat perturbatively only those parts of (23) that depend on α explicitly:

$$\mathcal{H}_l = \mathcal{U}_l + \alpha\mathcal{V}, \tag{28}$$

$$\mathcal{U}_l = \begin{pmatrix} d_+ & \chi_+^2 & 0 & 0 \\ \chi_+^2 & \tilde{d}_+ & 0 & 0 \\ 0 & 0 & d_- & \chi_-^2 \\ 0 & 0 & \chi_-^2 & \tilde{d}_- \end{pmatrix},$$

$$\mathcal{V} = \chi_+\chi_-\begin{pmatrix} 0 & 0 & 1 & 1 \\ 0 & 0 & 1 & 1 \\ 1 & 1 & 0 & 0 \\ 1 & 1 & 0 & 0 \end{pmatrix}.$$

For the eigenvalues of matrix $\eta\mathcal{U}_l$, we find the following simple expressions:

$$\begin{aligned} \lambda_{1,2}^+ &= l\left[2m_+ \pm \sqrt{l^2 + 2\chi_+^2}\right], \\ \lambda_{1,2}^- &= l\left[2m_- \pm \sqrt{l^2 + 2\chi_-^2}\right]. \end{aligned} \tag{29}$$

Eigenvalues of $\eta\mathcal{H}$ with nonzero imaginary part may appear around degeneracy points of $\eta\mathcal{U}_l$. In the trivial case, $\Delta m = 0$, the degeneracies may only appear when $\chi_-^2 = \chi_+^2$, i.e., at $z = 0$, which is the case studied above: the eigenvalues of matrix (23) are given by (25). As seen from Eq. (25), this does not lead to any instabilities as soon as $|\alpha| \leqslant 1$. In the following, we will assume $\Delta m \neq 0$. Equating the eigenvalues $\lambda_{1,2}^+$ and $\lambda_{1,2}^-$, we get for degeneracies $\lambda_1^+ = \lambda_2^-$ ($\Delta m > 0$) and $\lambda_2^+ = \lambda_1^-$ ($\Delta m < 0$) realized when $|z| \leqslant 2\Delta m^2$,

$$\rho_c(z) = \Delta m^2 - l^2 + \frac{z^2}{4\Delta m^2}. \tag{30}$$

Applying the perturbation theory for non-Hermitian operators [36], we find the first-order corrections to the degenerate eigenvalues. At $\rho = \rho_c$, these are

$$\Delta\lambda = \pm\frac{i\alpha l\chi_+\chi_-}{[(l^2 + 2\chi_+^2)(l^2 + 2\chi_-^2)]^{1/4}} \tag{31}$$

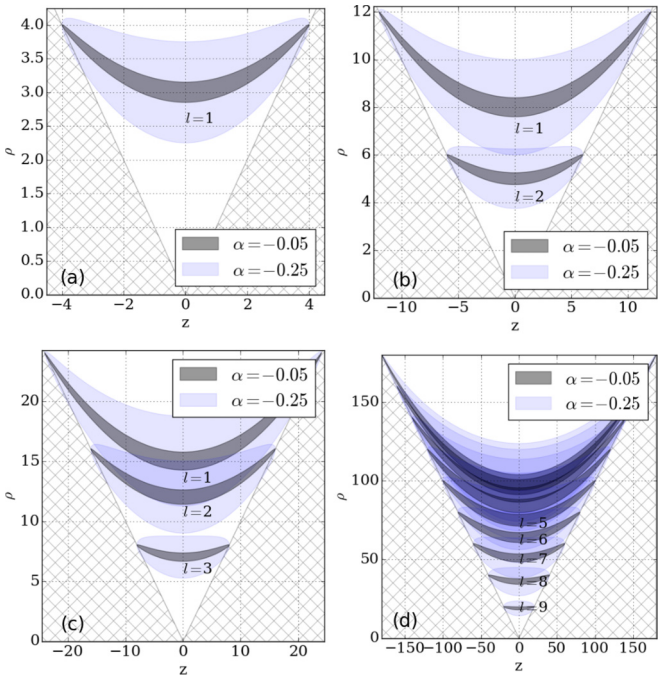

FIG. 3. Instability regions of topological spin Meissner (TSM) states with $|\Delta m| = 2$ (a), $|\Delta m| = 3$ (b), $|\Delta m| = 4$ (c), and $|\Delta m| = 10$ (d) as given by the analytical formulas (30) and (32). Dark and light blue areas are instability regions in parameter space (z,ρ) arising at different angular harmonics l for two different values of the parameter α: -0.05 and -0.2, correspondingly. The hatched area marks the region $|z| \geqslant \rho$ where solutions in the form of TSM states do not exist [see Eq. (13)].

and for $l \neq 0$, it leads to instability due to the appearance of an eigenvalue with a positive imaginary part.

Treating the deviation $\rho - \rho_c$ from ρ_c as a perturbation, we find the size of the instability interval $(-\Delta\rho, \Delta\rho)$ centered around ρ_c,

$$\Delta\rho = \left(\frac{8\alpha^2 \chi_+^2 \chi_-^2 \sqrt{l^2 + 2\chi_+^2}\sqrt{l^2 + 2\chi_-^2}}{l^2 + \chi_+^2 + \chi_-^2 + \sqrt{l^2 + 2\chi_+^2}\sqrt{l^2 + 2\chi_-^2}} \right)^{1/2}, \quad (32)$$

where χ_+, χ_- are evaluated using Eq. (10) at $\rho = \rho_c$.

One may check that the other two degeneracies, $\lambda_1^+ = \lambda_1^-$ and $\lambda_2^+ = \lambda_2^-$, which realize when $|z| \geqslant 2\Delta m^2$ do not lead to imaginary eigenvalues and, therefore, do not cause instabilities.

Formula (30) together with condition $|z| < \rho$ imply that the four half-vortices (1,0), (−1,0), (0,1), and (0,−1) have no instability regions, i.e., they are linearly stable for all values of ρ. The first nontrivial case arises for states with $|\Delta m| = 2$. Instability regions for states with $|\Delta m| = 2$, 3, 4, and 10 are shown in a parameter space of ρ versus z in Fig. 3.

We estimate the dynamical effect of the unstable mode on the distribution of the spinor components. Assuming the unstable mode dominates other modes but still can be treated as a perturbation around the stationary solution, we write

$$\varepsilon_\pm \approx [u_\pm e^{ilx - i\lambda_r t} + v_\pm^* e^{-ilx + i\lambda_r t}] e^{\lambda_i t}, \quad (33)$$

where we explicitly separated the real $\lambda_r = \mathrm{Re}\,\lambda$ and imaginary $\lambda_i = \mathrm{Im}\,\lambda$ parts of the eigenvalue causing the instability. Substituting (33) to the expressions for densities $|\phi_\pm|^2 = |\chi_\pm + \varepsilon_\pm(x,t)|^2$, we see that the growing unstable mode modulates the densities of the spinor components in the form of a propagating wave with a phase velocity $v = \lambda_r/l$. The real part λ_r can be estimated from expressions (29). At degeneracies $\lambda_1^+ = \lambda_2^- \equiv \lambda$ and $\lambda_2^+ = \lambda_1^- \equiv \lambda$, we find for the phase velocity at $\rho = \rho_c(z)$,

$$v = m_+ + m_- - \frac{z}{2\Delta m}. \quad (34)$$

Thus v is determined by the total angular momentum $m_+ + m_-$ of a TSM state.

We use the split step (Fourier) method to numerically analyze the dynamics of the unstable states. The (−1,1), (−2,2), and (−1,2) cases are shown in Fig. 4. The onset of unstable modes with a number of peaks or deeps is equal to the angular harmonics l, in agreement with the corresponding instability regions in Fig. 3. The instability develops as a wave of density modulations. The unstable modes with $l = 1$ and $l = 2$ around the state (−1,2) cause the density modulation to rotate with phase velocity $v \approx 1$, see Figs. 3(c) and 3(d). While density modulations in state (−1,2) move anticlockwise (increasing x), density modulations in state (−2,1) move clockwise in agreement with the opposite sign of the phase velocity in Eq. (34) (see Ref. [37]).

IV. CONSTANT-AMPLITUDE SPIN MEISSNER STATES IN PRESENCE OF TE-TM SPLITTING

We are now going to look at how the presence of a nonzero TE-TM splitting influences TSM states and the topological spin Meissner effect. It is convenient to eliminate the explicit dependence on x from the TE-TM splitting term, which is achieved through the substitution

$$\psi_\pm = \phi_\pm(x) e^{\mp i x}. \quad (35)$$

With this substitution, we get the following auxiliary system of equations, which takes a rotationally invariant form:

$$\begin{aligned} i\dot{\phi}_+ &= [\hat{D}_+ + |\phi_+|^2 + \alpha|\phi_-|^2]\phi_+ + \kappa\phi_-, \\ i\dot{\phi}_- &= [\hat{D}_- + |\phi_-|^2 + \alpha|\phi_+|^2]\phi_- + \kappa\phi_+, \end{aligned} \quad (36)$$

where $\hat{D}_\pm = 1 - \mu - \partial_x^2 \pm 2i\partial_x \pm \Omega$. The form of equation (36) is explicitly invariant under rotations, i.e., a shift of coordinate $\hat{\mathcal{R}}(\Delta x)\phi_\pm(x) = \phi_\pm(x + \Delta x)$.

In the linear regime and $\kappa \neq 0$, the stationary version of the system (36) is a linear system of equations with constant coefficients, which has solutions in the form of exponentials

$$\phi_\pm(x) = \chi_\pm e^{inx}, \quad \kappa \neq 0 \quad (37)$$

with the winding number n for both components and amplitudes

$$\chi_+ = \sqrt{\frac{\rho}{1+\xi^2}}, \quad \chi_- = \xi\sqrt{\frac{\rho}{1+\xi^2}}, \quad (38)$$

where $\xi \equiv \chi_-/\chi_+$ can take two values,

$$\xi = \xi_\pm, \quad \xi_\pm \equiv \frac{2n - \Omega}{\kappa} \pm \sqrt{1 + \left(\frac{2n - \Omega}{\kappa}\right)^2}. \quad (39)$$

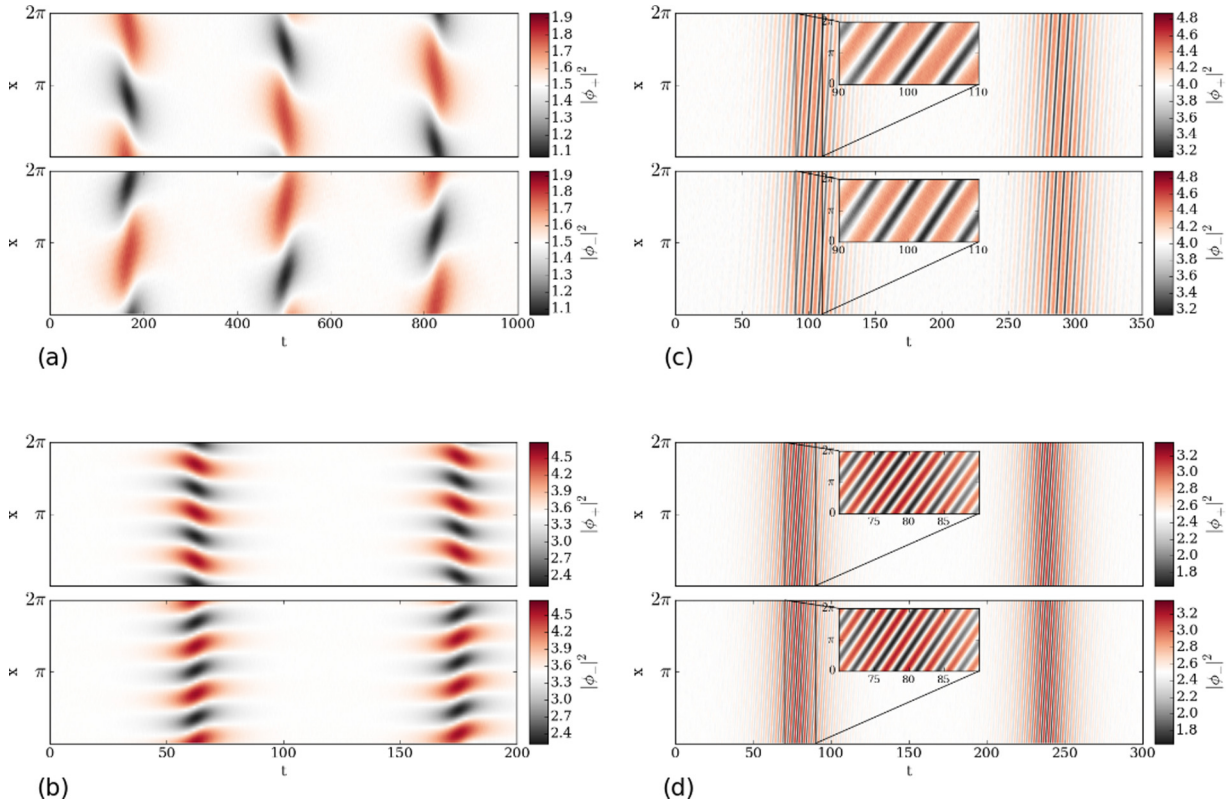

FIG. 4. Numerically calculated dynamics arising when the unstable states in the instability regions shown in Fig. 3 are distorted by a small initial perturbation. (a) $l = 1$ instability in state $(-1,1)$ at $\rho = 3$. (b) $l = 3$ instability in state $(-2,2)$ at $\rho = 7$. (c) $l = 1$ and (d) $l = 2$ instabilities in state $(m_+,m_-) = (-1,2)$ at $\rho = 8$ and $\rho = 5$, correspondingly. The onset of the modes with the number of peaks equal to the angular momentum l of the unstable mode is well visible, in agreement with Fig. 3. In all cases, $z = 0$ for each state, $\alpha = -0.05$ and TE-TM splitting is absent $\kappa = 0$. Video of the animated dynamics is available in Ref. [37].

Energies of the solutions (38) are

$$\mu = 1 + n^2 \pm \sqrt{(\Omega - 2n)^2 + \kappa^2}. \tag{40}$$

Note that the winding numbers in the $\psi_\pm$ representation [Eq. (1)] are given by

$$m_\pm = n \mp 1, \quad \Delta m = 2. \tag{41}$$

The linear spectrum (40) is plotted in Fig. 5 for the cases of zero ($\kappa = 0$) and nonzero ($\kappa = 0.1$) TE-TM splitting. The splitting of energy levels at $\Omega = \Omega_c \equiv 2n$ caused by TE-TM splitting is seen in Fig. 5(b). The avoided crossings arrange in a parabolic pattern $\mu(\Omega_c) \sim \Omega_c^2$ as given by formula (40).

We now look into the nonlinear case. The constant-amplitude solutions of the nonlinear system (36) have the same form (37) where the amplitudes (38) are defined by real roots of the fourth-order algebraic equation on ξ:

$$\kappa(\xi^4 - 1) - \rho(1 - \alpha)(\xi^3 - \xi) + 2(\Omega - 2n)(\xi^3 + \xi) = 0, \tag{42}$$

which, in general, may have 4, 2, or 0 real roots. The bifurcations between pairs of real and complex roots when changing the magnetic field and strength of TE-TM splitting κ can be traced in Fig. 6. The figure shows the evolution of the constant amplitude branches with changing strength of TE-TM splitting κ at a fixed nonlinearity $\rho = 3$. The TSM branches exist for small κ keeping their magnetic field-independent form of chemical potential. On increasing κ, the topological spin Meissner effect in the lower branch gradually comes to a naught acquiring a parabolic dependence on Ω, while the top branch disappears completely at high κ.

Although, the exact solutions can be found by solving Eq. (42), it is instructive to find their explicit expressions in

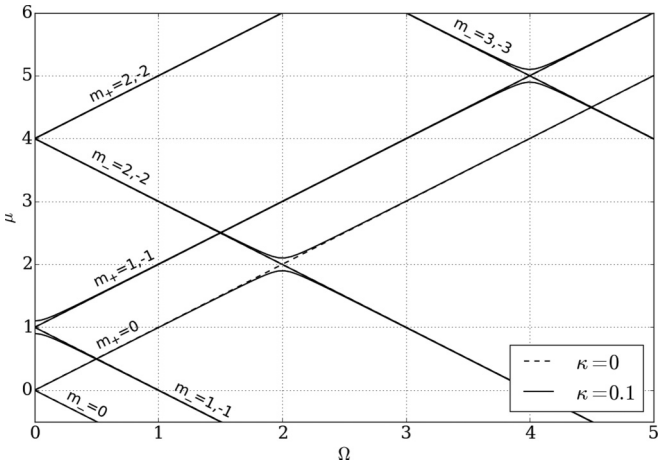

FIG. 5. Linear spectrum in presence (solid lines) and absence (dashed lines) of TE-TM splitting. TE-TM splitting results in anticrossings at $\Omega = \Omega_c \equiv 2n$, $n = 0, \pm 1, \ldots$ for branches $m_\pm = n \pm 1$, see Eq. (6).

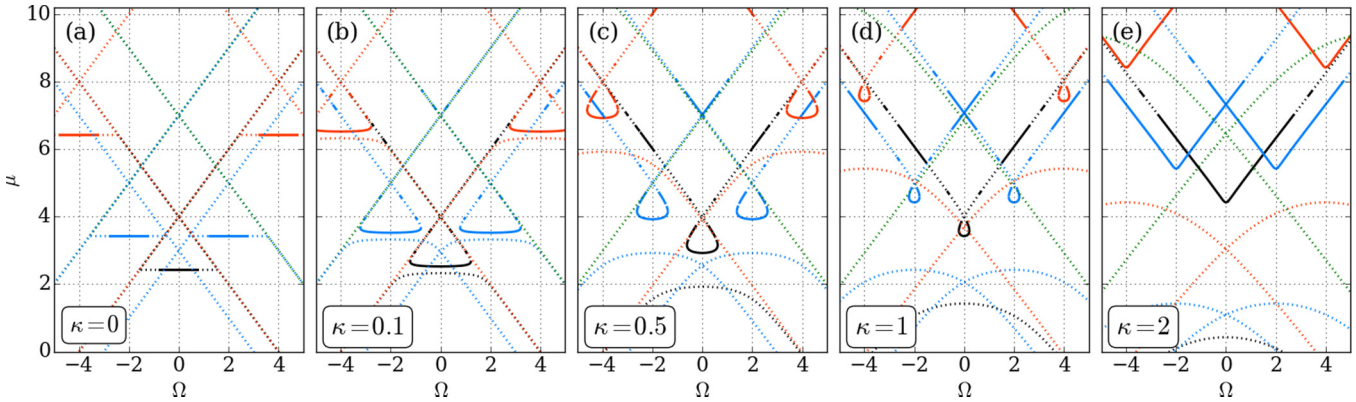

FIG. 6. The graphs show the evolution of constant-amplitude solutions of the system (1) with increasing TE-TM splitting for different values of the phase winding number m. Black, blue, red, and green lines correspond to the states with $|n| = 0$, 1, 2, and 3. TE-TM splitting parameter κ is increased from 0.0 (a) to 0.1 (b), 0.5 (c), 1.0 (d), and 2.0 (e). The nonlinearity parameters are $\rho = 3$ and $\alpha = -0.05$. The splitting of constant-amplitude TSM states into stable and unstable branches is visible in (b) when nonzero κ is introduced. For visibility purposes, unstable regions are marked by solid lines and stable regions are marked by dotted lines. Note that only constant-amplitude solutions are shown here.

the limit of small κ (see Ref. [37]). In the first order in κ, we find for TSM states $\Delta n = 0$,

$$\mu = \mu^{(0)} + \frac{\kappa\,\rho}{2\chi_+\chi_-} + O(\kappa^2), \tag{43}$$

where the zero-order term $\mu^{(0)}$ is given by (14) and $\chi_+\chi_- > 0$, $\chi_+\chi_- < 0$ are two distinct branches of solutions. The splitting of the TSM states $\Delta m = 2$ into symmetric ($\chi_+\chi_- > 0$) and antisymmetric ($\chi_+\chi_- < 0$) when a nonzero κ is introduced is shown in Fig. 7. In zero magnetic field and absence of interactions, $(-1,1)s$ and $(-1,1)a$ are the two lowest TE and TM modes in a ring, while higher-order states such as $(-2,0)s$, $(0,2)s$, $(-2,0)a$, and $(0,2)a$ are propagating TE and TM modes with nonzero wave vector. In the linear limit $\rho \to 0$,

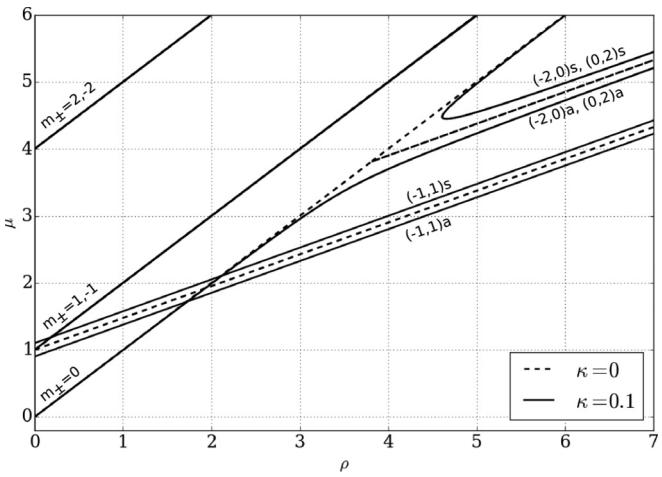

FIG. 7. Splitting of the spin Meissner states $\Delta m = 2$ under a nonzero κ: states $(-1,1)$, $(-2,0)$, and $(0,2)$ shown here split into symmetric ($\chi_+\chi_- > 0$) and antisymmetric ($\chi_+\chi_- < 0$) branches marked by "s" and "a" after the brackets with a pair of winding numbers (m_+,m_-). Dashed line and solid lines correspond to $\kappa = 0$ and $\kappa = 0.1$, respectively. Other parameters are $\alpha = -0.05$ and $\Omega = 0$. For simplicity, only constant-amplitude solutions are shown here.

the splitting of the $(-1,1)$ state is the avoided crossings given by linear spectrum (40) and shown in Fig. 5.

We analyze analytically the stability of the constant-amplitude TSM states solving perturbatively the eigenvalue problem for operator $\hat{L} = \eta\hat{H}$, where operator $\hat{H}$ is given in Appendix C. Because the constant-amplitude TSM states are split in two branches when nonzero κ is present, perturbation expansion for eigenvalues of the operator $\hat{L} = \hat{L}_0 + \kappa\hat{L}_1 + O(\kappa^2)$ will involve powers of $\kappa^{1/2}$,

$$\lambda = \kappa^{1/2}[\lambda_0 + O(\kappa)], \tag{44}$$

where for λ_0 we find (see details in Appendix C)

$$\lambda_0^2 = \mp 2(1-\alpha)\sqrt{\rho^2 - z^2} \tag{45}$$

for states $\chi_+\chi_- > 0$ and $\chi_+\chi_- < 0$, correspondingly. Therefore, for $\kappa > 0$, the state with $\chi_+ = \chi_-$ is unstable and state $\chi_+ = -\chi_-$ is stable (for $\kappa < 0$ the situation reverses). For the unstable mode with eigenvalue given by (45), we find

$$\varepsilon_\pm \sim \pm\chi_\pm e^{inx} = \pm\phi_\pm(x), \tag{46}$$

i.e., the unstable mode (46) results in a homogeneous change of density distributions of the spinor components.

We compare the theoretical estimate (44) and (45) of the imaginary part of the eigenvalue λ causing the instability to its exact value obtained by a numerical diagonalization of matrix (47) for different angular harmonics l. The results of comparison for the dependence of Imλ on κ are presented in Figs. 8(a) and 8(b) for two different values of nonlinearity parameter ρ. The theoretical results (44) and (45) obtained by perturbation expansion agree with the numerical calculation for $l = 0$ at small κ. A small region of instability caused by angular harmonics $l = 1$ is also visible in Fig. 8(a) for small values of κ and is caused by the instability region $l = 1$ on Fig. 3(a) [see Fig. 3(a) at $\rho = 3$]. With increasing strength of TE-TM splitting, a state becomes unstable with respect to several harmonics simultaneously.

In our numerical analysis of stability we solve the eigenvalues problem of the operator $\hat{\eta}\hat{\mathcal{H}}_l(\kappa)$, where

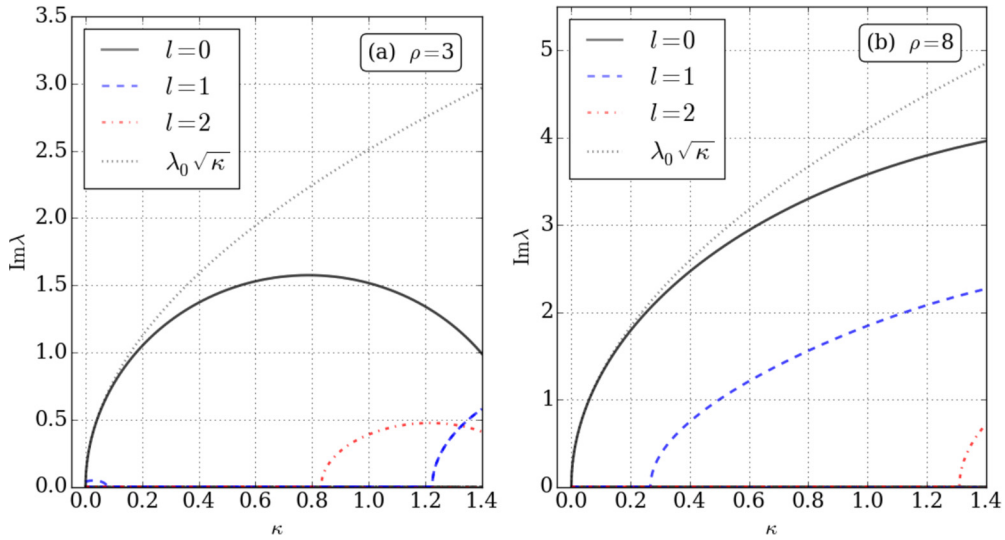

FIG. 8. Imaginary part of the eigenvalues of matrix (47) as a function of κ, evaluated at the unstable branch of the state $(-1,1)$ and $\Omega = 0$. Black, dashed and dashed-dotted lines correspond to instabilities caused by angular harmonics $l = 0$, 1, and 2, respectively. Dotted line is the theoretical estimate given by the first term in formula (44) with (45).

(see Appendix B for details)

$$\hat{\mathcal{H}}_l(\kappa) = \begin{pmatrix} d_+ & \chi_+^2 & \alpha\chi_+\chi_- + \kappa & \alpha\chi_+\chi_- \\ \chi_+^2 & \tilde{d}_+ & \alpha\chi_+\chi_- & \alpha\chi_+\chi_- + \kappa \\ \alpha\chi_+\chi_- + \kappa & \alpha\chi_+\chi_- & d_- & \chi_-^2 \\ \alpha\chi_+\chi_- & \alpha\chi_+\chi_- + \kappa & \chi_-^2 & \tilde{d}_- \end{pmatrix}, \tag{47}$$

$\hat{\eta}$ was defined above and the diagonal elements $d_\pm$,$\tilde{d}_\pm$ are given by

$$d_\pm \equiv l^2 + 2lm_\pm + \chi_\pm^2 + [-\mu + m_\pm^2 + \chi_\pm^2 + \alpha\chi_\mp^2 \pm \Omega], \tag{48}$$

$$\tilde{d}_\pm \equiv l^2 - 2lm_\pm + \chi_\pm^2 + [-\mu + m_\pm^2 + \chi_\pm^2 + \alpha\chi_\mp^2 \pm \Omega]. \tag{49}$$

Matrix (47) is a generalization of (23) to nonzero κ.

The solution is spectrally unstable if there is at least one eigenvalue with positive imaginary part $\mathrm{Im}\,\lambda > 0$. The results of the stability analysis are shown in Fig. 6. Dashed lines mark stable regions and solid lines mark unstable regions (stability analysis with respect to the individual harmonics l can be found in Ref. [37]). As seen from Fig. 6, the constant-amplitude TSM states are split into stable (bottom) and unstable (top) branches, in agreement with (45). At $\kappa = 0$, the instability is caused by angular harmonics $l = 1$, which corresponds to the instability region shown in Fig. 3(a), while for nonzero κ the $l = 0$ mode appears as seen in Fig. 8(a).

Finally, we analyze the dynamics of instability arising due to the unstable mode in the presence of TE-TM splitting. The results of our time-dependent numerical calculations are shown in Fig. 9. As seen from the figure, the presence of TE-TM splitting leads to a homogeneous instability mode in agreement with formula (46).

V. SYMMETRY-BREAKING SPIN MEISSNER STATES

In the previous section, we focused our attention to the TSM states with the constrained phase winding numbers $\Delta m = 2$: these are constant-amplitude solutions at nonzero TE-TM splitting. In this section, we will investigate the fate of the more general states (3) with arbitrary m_+, m_-. It turns out that solutions with $\Delta m \neq 2$ do not disappear in the presence of nonzero κ but instead develop inhomogeneous profiles.

At $\kappa = 0$, constant amplitude solutions of the auxiliary system of equations (36) are expressed via solutions (3) studied in Sec. III,

$$\phi_\pm(x) = \chi_\pm e^{i(m_\pm \pm 1)x} \tag{50}$$

Important aspects of the continuation of TSM states from $\kappa = 0$ to $\kappa \neq 0$ can be understood if we consider changes in the symmetry properties of the model equations and of the solutions themselves. Equations (36) with $\kappa = 0$ are invariant

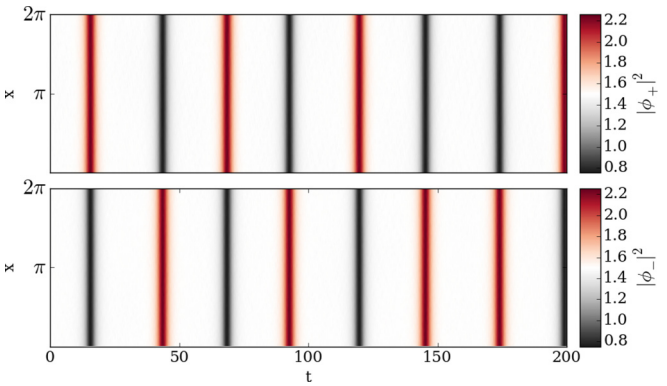

FIG. 9. Numerically calculated dynamics of instability arising when unstable state $(-1,1)$ at $\rho = 3$, $\Omega = 0$ is distorted by a small initial perturbation in the presence of TE-TM splitting $\kappa = 0.1$. The onset of $l = 0$ mode is visible in agreement with (a). Video of the animated dynamics is available in Ref. [37].

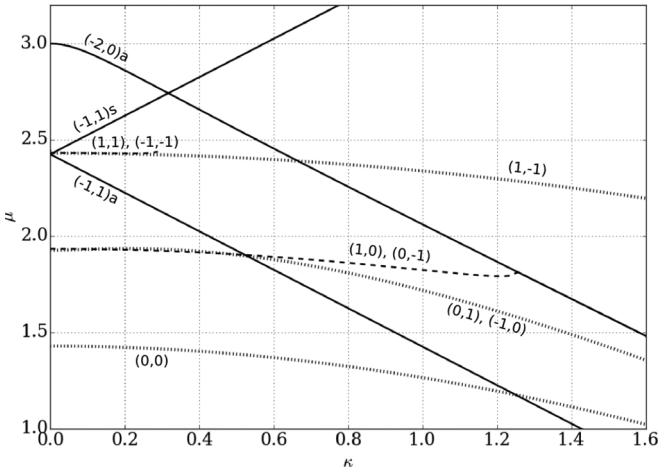

FIG. 10. Numerical continuation of states in parameter κ to the region of nonzero TE-TM splitting. Solid lines mark constant amplitude solutions, dashed and dotted lines mark symmetry-breaking states. Splitting of the state $(-1,1)$ into two branches can be seen. Contrary to the constant amplitude states, symmetry-breaking states do not split into branches but develop inhomogeneous density profiles. The $(1,1)$, $(-1,-1)$ develop instabilities at $\kappa \approx 0.3$, which lead to breaking of the branch. Other parameters are $\alpha = -0.05$ and $\Omega = 0$.

under the following three transformations: rotation of the total phase of the spinor, rotation of the relative phases of the spinor components and shift of the azimuthal coordinate x. However, not all of these operations are independent. Consider a shift of the coordinate $x \to x + \Delta x$,

$$\hat{\mathcal{R}}(\Delta x)\begin{pmatrix}\chi_+ e^{in_+x}\\ \chi_- e^{in_-x}\end{pmatrix} = e^{i\Delta x(m_+ + m_-)/2}\begin{pmatrix}\chi_+ e^{in_+x - i\delta/2}\\ \chi_- e^{in_-x + i\delta/2}\end{pmatrix}, \quad (51)$$

where $\delta = (\Delta m - 2)\Delta x$ and $n_\pm = m_\pm \pm 1$. Thus the shift of the coordinate of the constant-amplitude solutions (50) is equivalent to a rotation of the total phase, if $\Delta m = 2$, or, rotation of both total and relative phases, if $\Delta m \neq 2$. When TE-TM splitting is not zero, $\kappa \neq 0$, then the symmetry of the model with respect to the shift of the relative phase is broken. This affects very differently solutions with $\Delta m = 2$ and $\Delta m \neq 2$. Those with $\Delta m = 2$ remain invariant with respect to rotations in x, which are equivalent to the corresponding shift in the still present total phase. Meanwhile, former $\Delta m \neq 2$ solutions develop inhomogeneous density profiles as their rotational symmetry becomes broken. Thus, for $\kappa \neq 0$, $\Delta m = 2$ solutions have one broken symmetry (total phase) and one Goldstone mode associated with it and $\Delta m \neq 2$ solutions have two broken symmetries and two Goldstone modes. While for $\kappa = 0$, both types of solutions have two broken symmetries (in the total and relative phases). Because the number of Goldstone bosons does not change for $\Delta m \neq 2$ solutions, they do not branch as we introduce $\kappa \neq 0$, while $\Delta m = 2$ split into branches, see Fig. 10.

Numerical continuation of the solutions (3) in parameter κ to the domain of nonzero TE-TM splitting is presented in Fig. 10 for a fixed nonlinearity parameter $\rho = 3$. At $\kappa = 0$, the energies of the solutions are given by Eqs. (8), (9), and (14), see also a cross section of Fig. 1(b) at $\rho = 3$. With increasing TE-TM splitting parameter the solutions

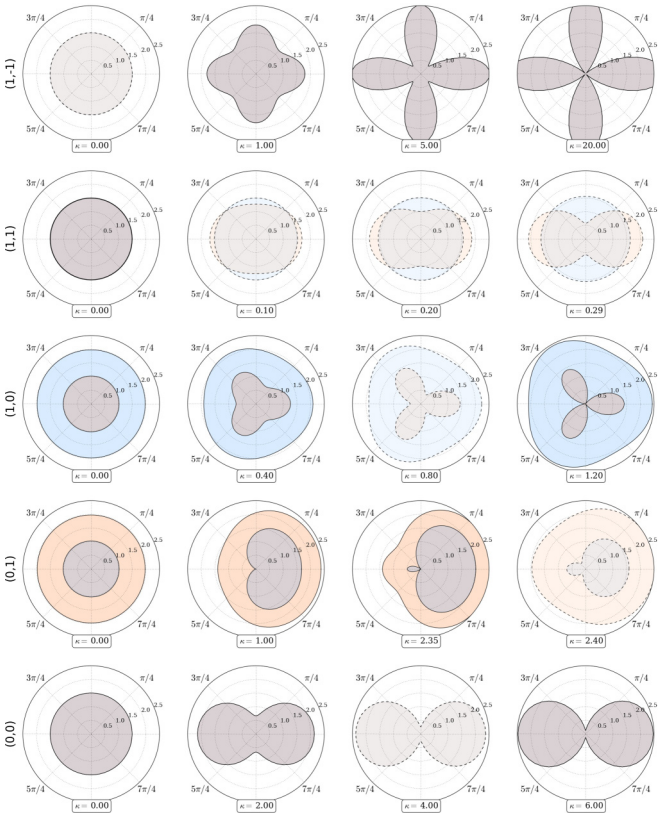

FIG. 11. Numerical continuation of TSM states given by Eqs. (10) at $\kappa = 0$ to the domain of nonzero TE-TM splitting. The evolution of the densities of the spinor components of symmetry-breaking states during the continuation is shown with the parameter κ increasing from left to right. Polar plots correspond to the branches of the symmetry-breaking states in Fig. 10 with the same nonlinearity strength $\rho = 3$. Parameters of the calculations are $\Omega = 0$ and $\alpha = -0.05$. States $(-1,0)$ and $(0,-1)$ are not shown as they evolve in the same way as $(0,1)$ and $(1,0)$, respectively, with spinor components interchanged. Dashed lines and fainter colors mark unstable states.

with winding numbers (m_+,m_-), $\Delta m \neq 2$ continue to exist developing inhomogeneous density profiles. Splitting of the constant amplitude states with $\Delta m = 2$ into two branches is also visible in Fig. 10. Contrary to the constant amplitude states, symmetry breaking states do not split into branches. Indeed, as can be seen from formula (51), states with different relative phase of the spinor components at $\kappa = 0$ seed the same solution at $\kappa \neq 0$, apart from the coordinate shift and a common phase factor. Snapshots of the evolution of densities of the spinor components under continuously changing κ are shown on Fig. 11.

Symmetry-breaking states can be classified according to which states they can be continued from by increasing the TE-TM splitting κ from zero because they inherit topological properties of the seeding solutions, i.e., their two phase winding numbers. Indeed, the two topological invariants, which could be used to characterize a symmetry-breaking TSM state, are

$$\frac{1}{2\pi i}\int_0^{2\pi} \frac{\partial_x \phi_\pm}{\phi_\pm} dx, \quad (52)$$

and coincide with $m_\pm$ of the constant-amplitude TSM state at $\kappa = 0$ to which it can be continued given that neither of the components turned to zero during the continuous transformation.

To analyze analytically TSM states with broken rotational symmetry in presence of TE-TM splitting, we use a perturbative approach and consider a small distortion $\varepsilon_\pm(x)$ of the shape of the TSM state (10):

$$\phi_\pm(x) = [\chi_\pm + \kappa\varepsilon_\pm(x) + O(\kappa^2)]e^{i(m_\pm \pm 1)x} \tag{53}$$

$$\mu = \mu^{(0)} + \kappa\mu^{(1)} + O(\kappa^2), \tag{54}$$

where $\varepsilon_\pm(x)$ are complex functions and $\chi_\pm$ are amplitudes of the TSM state at $\kappa = 0$. Substituting into (36) we get a system of equations on $\varepsilon_\pm(x)$,

$$\begin{aligned} &-\varepsilon_\pm'' - 2im_\pm\varepsilon_\pm' + \chi_\pm^2(\varepsilon_\pm + \varepsilon_\pm^*) + \alpha\chi_\pm\chi_\mp(\varepsilon_\mp + \varepsilon_\mp^*) \\ &\quad = \mu^{(1)}\chi_\pm - e^{\pm i(\Delta m - 2)x}\chi_\mp. \end{aligned} \tag{55}$$

Assuming $\Delta m \neq 2$, we may seek for solutions of (55) in the form

$$\varepsilon_\pm = A_\pm e^{\pm i(\Delta m-2)x} + B_\pm e^{\mp i(\Delta m-2)x} + C_\pm, \tag{56}$$

where coefficients $A_\pm$, $B_\pm$, and $C_\pm$ can be chosen real. Substituting into (55) and using the normalization condition, we get two decoupled systems of equations:

$$\hat{\mathcal{H}}_{\Delta m-2}\mathbf{W} = \mathbf{R}, \tag{57}$$

$$Q\mathbf{C} = 0, \tag{58}$$

where $\mathbf{W} = (A_+, B_+, A_-, B_-)^T$, $\mathbf{C} = (C_+, C_-, \mu^{(1)})^T$, $\mathbf{R} = (-\chi_-, 0, -\chi_+, 0)^T$, and matrix $\hat{\mathcal{H}}_{\Delta m-2}$ is given by Eq. (23) for $l = \Delta m - 2$ and

$$Q = \begin{pmatrix} 2\chi_+^2 & 2\alpha\chi_+\chi_- & -\chi_+ \\ 2\alpha\chi_+\chi_- & 2\chi_-^2 & -\chi_- \\ \chi_+ & \chi_- & 0 \end{pmatrix}. \tag{59}$$

The determinant of matrix Q is $\det Q = 4\chi_+^2\chi_-^2(1-\alpha)$, which is nonzero as $\chi_-, \chi_+ \neq 0$. Therefore, for the TSM states, only a trivial solution to the system (58) exists, i.e., $C_1 = C_2 = \mu^{(1)} = 0$. Because $\mu^{(1)} = 0$ and $\mu^{(0)}$ does not change with the magnetic field, the energy μ of the symmetry-breaking solutions induced by TSM states is also independent of the magnetic field, i.e., *symmetry-breaking solutions induced by topological spin Meissner states remain spin Meissner states*, at least in the first order in TE-TM splitting. Therefore, from (14) for symmetry-breaking TSM states in the presence of TE-TM splitting, we have

$$\mu = \tfrac{1}{2}[m_+^2 + m_-^2 + \rho(1+\alpha)] + O(\kappa^2). \tag{60}$$

To find the density profiles of the symmetry-breaking solutions, we solve system (57). For small κ, perturbative solutions (56) are in good agreement with our numerical calculations (see Ref. [37] for comparison between the theoretical and numerical results).

The influence of TE-TM splitting on the topological spin Meissner effect is shown in Fig. 12. As seen from the figure, the energies of the symmetry-breaking TSM states depend weakly on the magnetic field even in the presence of significant TE-TM splitting $\kappa = 1$. Notice that the spin Meissner effect is not exact for states with nonzero net angular momentum $m_+ + m_-$, while it holds better for states with zero angular momentum such as (0,0) and (1,−1).

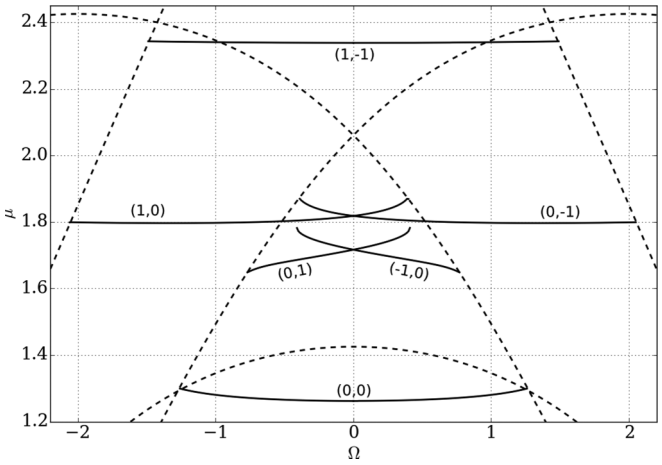

FIG. 12. Topological spin Meissner effect in the presence of TE-TM splitting. As seen from the figure, the energies of symmetry-breaking TSM states (solid lines) depend weakly on the magnetic field even in the presence of significant TE-TM splitting $\kappa = 1$ as in the calculation presented here. Note that the spin Meissner effect is not exact for states with nonzero net angular momentum $m_+ + m_-$ while it holds better for states with zero angular momentum such as (0,0) and (1,−1). Dashed lines mark constant-amplitude solutions. Nonlinearity parameters $\rho = 3$ and $\alpha = -0.05$.

Studies of topological spin Meissner effect in half-vortices (−1,0) and (1,0) are shown in Figs. 13(a) and 13(b). As seen from the figure, the magnetic field is balanced by the densities of the spinor components of a vortex state, with the energy of the state remaining nearly constant (cf. Fig. 12). Figures 12(a) and 12(b) show polar plots of the numerically calculated densities $|\phi_+|^2$ and $|\phi_-|^2$ for a fixed nonlinearity parameter $\rho = 3$. Dashed lines and fainter colors mark spectrally unstable states. The other two half-vortices, (0,1) and (0,−1) coincide with (1,0) and (−1,0) when two circular polarizations are interchanged and the direction of the magnetic field is reversed.

As seen from the analytical formula (56), quantity $\Delta m - 2$ defines the order of the discrete rotational symmetry in the density distribution of the states (i.e., the number of peaks or deeps): in (1,0) and (0,−1) it has a threefold rotational symmetry, while in states (0,1) and (−1,0) the density distribution has "onefold" symmetry (i.e., no rotational symmetry). The evolution of numerically calculated density distributions for a higher-order state (4,−4) with changing TE-TM splitting parameter κ is shown in Fig. 14. Due to $|\Delta m - 2| = 10$, its density distribution is tenfold rotationally symmetric.

We investigate the stability of the symmetry-breaking states numerically evaluating the eigenvalues of the discretized Hessian matrix [the continuous version of the Hessian matrix is given by Eq. (C2) in Appendix C]. The unstable states resulting from this analysis are marked by dashed lines and faint colors in Figs. 13(a) and 13(b). No instabilities were found among the configurations displayed in Fig. 14. We analyzed the unstable states of half-vortices marked by dashed lines and faint colors in Fig. 13. The arising dynamics when an

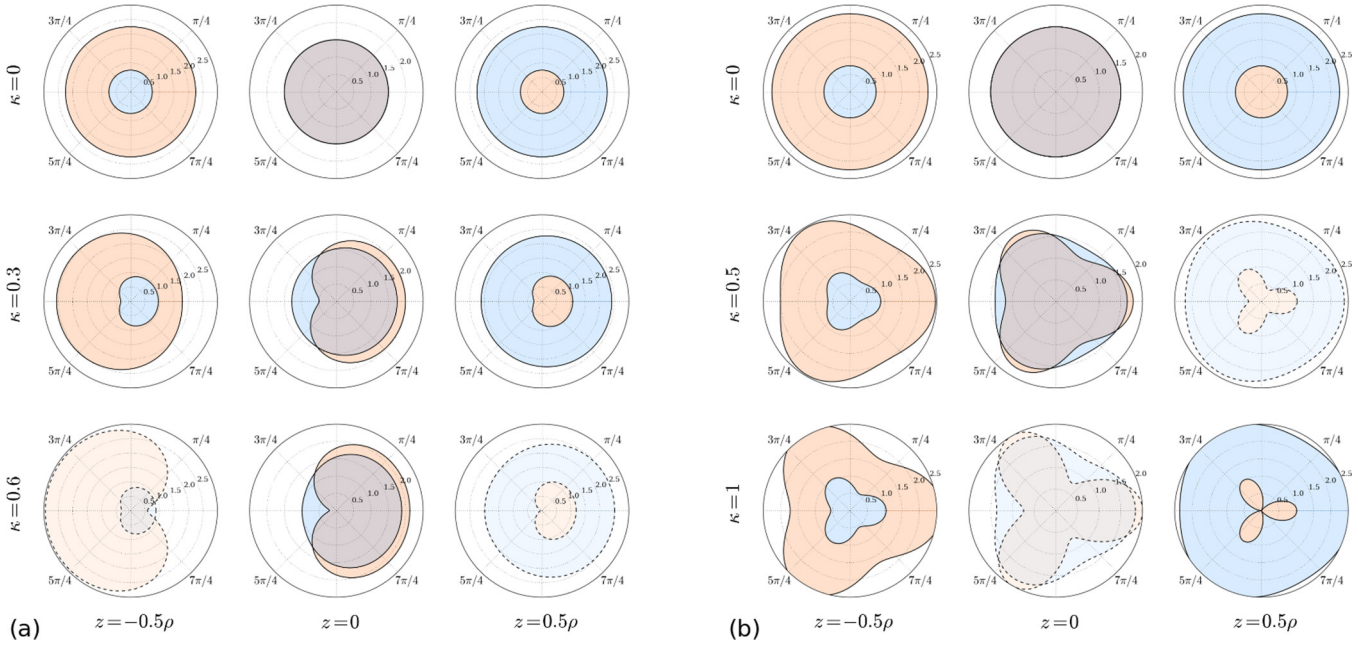

FIG. 13. Topological spin Meissner effect in half-vortices $(-1,0)$ (a) and $(1,0)$ (b): the effect of magnetic field is balanced by the changing densities of the spinor components of a vortex state, keeping the energy of the state nearly constant (see Fig. 12). Polar plots of numerically calculated density distributions are presented. Pink and blue colors represent densities $|\phi_+|^2$ and $|\phi_-|^2$, correspondingly. TE-TM splitting κ takes values, from top to bottom: 0, 0.3, and 0.6 in (a) and 0, 0.5, and 1.0 in (b). The magnetic field is given by $z/\rho = -0.5$, 0, and 0.5 from left to right, with z defined by Eq. (11). Nonlinearity parameters $\rho = 3$ and $\alpha = -0.05$. Dashed lines and fainter colors mark unstable states.

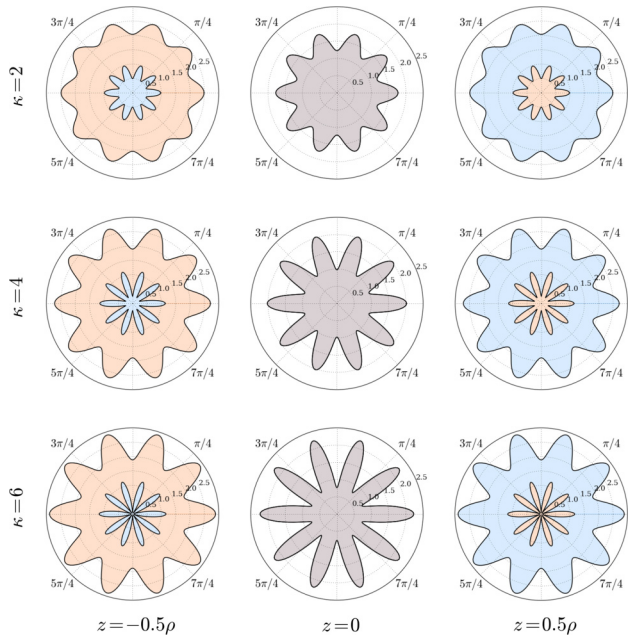

FIG. 14. Numerically continued symmetry-breaking TSM state $(4,-4)$ of higher-order rotational symmetry. Pink and blue colors represent densities $|\phi_+|^2$ and $|\phi_-|^2$, correspondingly. The values of κ are 2, 4, and 6 from top to bottom. Magnetic field is given by $z/\rho = -0.5$, 0, and 0.5 from left to right, with z defined by Eq. (11). Balancing of the magnetic field by density distributions of the spinor components in a polarization vortex (topological spin Meissner effect) is seen here. This leads to all states having energies independent of the value of the magnetic field. Nonlinearity parameters $\rho = 3$ and $\alpha = -0.05$. All of the displayed configurations were found to be stable with respect to linear perturbations.

unstable state is disturbed by a small perturbation is shown in Fig. 15. As seen from the figure, in the initial stage, the densities patterns are nearly constant as it takes time for the instability to develop. In the next stage when instability has grown large enough, quasiperiodic patterns appear, which indicate an onset of propagating waves that modulate the densities of the circular polarized components. Videos of the propagating density modulations are available in Ref. [37].

VI. DISCUSSION

To conclude, we have shown that an exciton-polariton condensate placed in a trap of nonsimply connected geometry may exhibit states whose energies are independent of the applied magnetic field. The properties of these states are dictated by the topology of the condensate wave function, i.e., two phase winding numbers of its spinor components. We analyzed the stability of these topological spin Meissner states and indicated the range of parameters where such states may exist and are stable. These findings helped us shed light onto the properties of half-vortices in a ring and gave us a clue in the understanding of the recent experiments. We analyzed the effect of TE-TM splitting on the topological spin Meissner states and found that stable states exist even in the presence of significant TE-TM splitting strengths. Finally, we found that a certain class of TSM states exist which breaks rotational symmetry in the presence of TE-TM splitting by developing inhomogeneous densities.

The range of parameters discussed in this paper can be reached experimentally. Depending on the size of the ring and

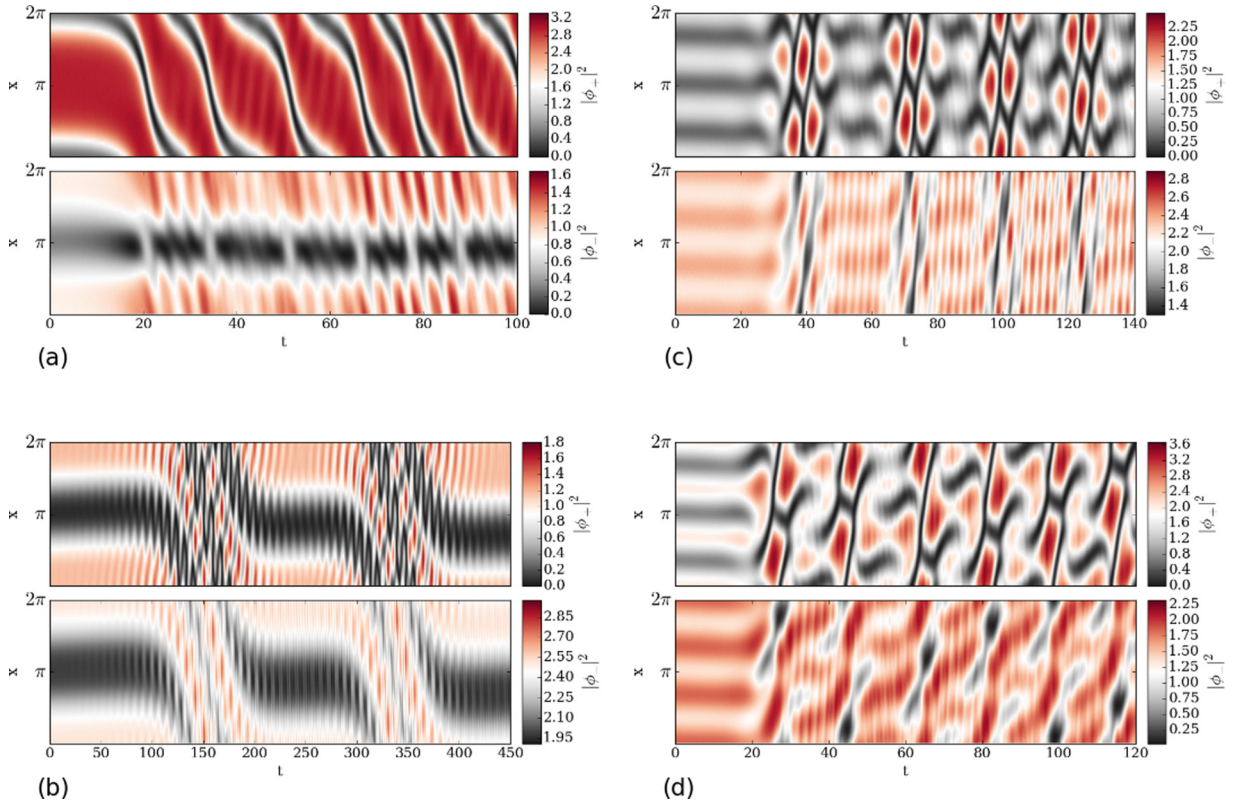

FIG. 15. Dynamics of instabilities arising when the unstable half-vortices shown in Fig. 13 are distorted by a small initial perturbation: state $(-1,0)$ at (a) $z/\rho = -0.5$, $\kappa = 0.6$ and (b) $z/\rho = 0.5$, $\kappa = 0.6$ (b) with the density profile in Fig. 13(a) and state $(1,0)$ at (c) $z/\rho = 0.5$, $\kappa = 0.5$ and (d) $z/\rho = 0$, $\kappa = 1$ with the density profile in Fig. 13(b). Videos of animated dynamics are available in Ref. [37].

detuning, the characteristic energy $\hbar^2/2m^*R^2$ may be varied in a broad range of energies. For a ring diameter 10 μm, the unit energy can vary from 4 to 40 μeV, depending on the detuning. Therefore both small $\Omega \sim 10$ and higher values are well accessible in experiments. The effect of TE-TM splitting can be made significant, if desired. In a 1-μm waveguide, TE/TM splitting can be as high as $\sim$1 meV [31,38], which allows to reach $\kappa \sim 10$ and even $\kappa \sim 100$, in normalized units. On the other hand, κ can be made negligibly small by choosing larger ring widths, by controlling detuning [39] and the properties of the distributed Bragg reflector [40].

ACKNOWLEDGMENTS

This work is supported under the project RFMEFI58715X0020 of the Federal Targeted Programme Research and Development in Priority Areas of Development of the Russian Scientific and Technological Complex for 2014-2020 of the Ministry of Education and Science of Russia. We acknowledge support from the European Commission FP7 LIMACONA 612600 and H2020 EU project 691011 SOLIRING. I.A.S. acknowledges support from the Singaporean Ministry of Education under AcRF Tier 2 Grant MOE2015-T2-1-055 and from Rannis excellence grant 163082-051 "2D transport in the regime of strong light-matter coupling." D.V.S. acknowledges support from the Leverhulme trust.

APPENDIX A: TE-TM SPLITTING IN MICROCAVITY RING RESONATOR

The TE-TM splitting of the linear polarization in quasi-one-dimensional microcavities may have different physical origins such as the difference in reflection coefficients for TE and TM polarizations in Bragg mirrors [40], the anisotropy caused by thermal expansion [38] and the influence of the boundaries [31].

The simpler case of k-independent TE-TM splitting may arise due to an anisotropy present in the system such as deformation due to a thermal stress [38] or difference in boundary conditions for electric and magnetic fields at the cavity-to-air interface [31]. Assuming a homogeneously distributed asymmetry with the axis aligned along the radial/azimuthal direction of the ring, for the polaritons coupled to the TE and TM modes, the TE-TM Hamiltonian acting on the spinor wave function $(\psi_r(\varphi,t),\psi_\varphi(\varphi,t))^T$,

$$\hat{H}_{\text{TE-TM}} = \begin{pmatrix} -\Delta & 0 \\ 0 & \Delta \end{pmatrix}, \tag{A1}$$

where 2Δ is the energy splitting for polarizations aligned along the radial and azimuthal directions. Transforming to the basis of circular polarizations, we get the Hamiltonian

$$\hat{H}_{\text{TE-TM}} = \begin{pmatrix} 0 & \Delta\, e^{-2i\varphi} \\ \Delta\, e^{2i\varphi} & 0 \end{pmatrix} \tag{A2}$$

acting on the wave function $(\psi_+(\varphi,t),\psi_-(\varphi,t))^T$. Here, $\psi_\pm = (\psi_x \mp i\psi_y)/\sqrt{2}$ are components of a spinor $\psi = \psi_+\hat{e}_+ + \psi_-\hat{e}_-$ in the circular polarization basis with vectors $\hat{e}_\pm = (\hat{e}_x \pm i\hat{e}_y)/\sqrt{2}$. The TE-TM splitting Hamiltonian in the form (A2) was established in work [23] to describe the polarization splitting of an exciton-polariton condensate in a one-dimensional ring interferometer.

The k-dependent TE-TM splitting arises due to the property of distributed Bragg reflectors to have slightly different angular dispersions for TE and TM polarizations [40]. This makes microcavity polaritons polarized longitudinally and transversely to their propagation direction to acquire different dispersion relations. In the effective mass approximation, the k-dependent TE-TM splitting can be described by introducing two masses $m_{\rm TM}$ and $m_{\rm TE}$ for polaritons polarized longitudinally (TM mode) and transversely (TE mode) with respect to the in-plane $\mathbf{k}$ vector. In a narrow ring resonator this type of TE-TM splitting becomes effectively independent of the wave number k_φ along the ring, as long as $k_r \gg k_\varphi$ is satisfied. Indeed, consider an exciton-polariton condensate confined in a ring trap of radius R and width ΔR. With account of k-dependent TE-TM and Zeeman splittings, it can be described by a system of coupled spinor Gross-Pitaevskii equations (cf. Refs. [27,30,39,41]):

$$\begin{aligned} i\hbar\frac{\partial\Psi_+}{\partial t} &= -\frac{\hbar^2}{2m^*}\nabla^2\Psi_+ + (\alpha_1|\Psi_+|^2 + \alpha_2|\Psi_-|^2)\Psi_+ \\ &\quad + \frac{1}{2}g_{\rm eff}\mu_B B\,\Psi_+ + \beta(\partial_x - i\partial_y)^2\Psi_- \\ i\hbar\frac{\partial\Psi_-}{\partial t} &= -\frac{\hbar^2}{2m^*}\nabla^2\Psi_- + (\alpha_1|\Psi_-|^2 + \alpha_2|\Psi_+|^2)\Psi_- \\ &\quad - \frac{1}{2}g_{\rm eff}\mu_B B\,\Psi_- + \beta(\partial_x + i\partial_y)^2\Psi_+, \end{aligned} \tag{A3}$$

where $\beta = \hbar^2(m_{\rm TE}^{-1} - m_{\rm TM}^{-1})/4$ is a parameter describing TE-TM splitting, $m^* = 2m_{\rm TE}m_{\rm TM}/(m_{\rm TE} + m_{\rm TM})$ is the effective mass, and $g_{\rm eff}$ is the effective exciton-polariton g factor, μ_B is the Bohr magneton, B is the applied magnetic field, and $\alpha_1 = U_0$ and $\alpha_2 = U_0 - 2U_1$ are parameters characterizing polariton-polariton interactions. In the limit of a narrow ring, we may use the adiabatic approximation and separate the radial dependence of the wave function, $\Psi_\pm(r,\varphi,t) = \zeta(r)\psi_\pm(\varphi,t)$, where $\zeta(r)$ is the normalized ground-state wave function in the radial direction, satisfying the stationary Schrödinger equation

$$\frac{\hbar^2}{2m^*}\left(-\partial_r^2 - \frac{1}{r}\partial_r + \frac{1}{r^2}\right)\zeta(r) = E\zeta(r).$$

Neglecting lower-order derivatives in r we arrive to the following 1D model:

$$\begin{aligned} i\hbar\frac{\partial\psi_+}{\partial t} &= -\frac{\hbar^2}{2m^*R^2}\frac{\partial^2}{\partial\varphi^2}\psi_+ + (\tilde{\alpha}_1|\psi_+|^2 + \tilde{\alpha}_2|\psi_-|^2)\psi_+ \\ &\quad + \frac{1}{2}g_{\rm eff}\mu_B B\,\psi_+ + \tilde{\beta}e^{-2i\varphi}\psi_- \\ i\hbar\frac{\partial\psi_-}{\partial t} &= -\frac{\hbar^2}{2m^*R^2}\frac{\partial^2}{\partial\varphi^2}\psi_- + (\tilde{\alpha}_1|\psi_-|^2 + \tilde{\alpha}_2|\psi_+|^2)\psi_- \\ &\quad - \frac{1}{2}g_{\rm eff}\mu_B B\,\psi_- + \tilde{\beta}e^{2i\varphi}\psi_+ \end{aligned} \tag{A4}$$

with effective parameters $\tilde{\alpha}_1, \tilde{\alpha}_2$, and $\tilde{\beta}$, which are connected to α_1, α_2, and β via parameters of the ring. Note that the TE-TM splitting Hamiltonian obtained in Eq. (A4) is of the same form as given by the k-independent TE-TM splitting (A2).

Introducing dimensionless units by rescaling the quantities entering Eqs. (A2) and (A4) to unit energy $E_0 \equiv \hbar^2/2m^*R^2$, we obtain

$$\begin{aligned} i\dot{\psi}_+ &= -\partial_\varphi^2\psi_+ + (|\psi_+|^2 + \alpha|\psi_-|^2)\psi_+ \\ &\quad + \Omega\psi_+ + \kappa e^{-2i\varphi}\psi_- \\ i\dot{\psi}_- &= -\partial_\varphi^2\psi_- + (|\psi_-|^2 + \alpha|\psi_+|^2)\psi_- \\ &\quad - \Omega\psi_- + \kappa e^{2i\varphi}\psi_+, \end{aligned} \tag{A5}$$

where $\alpha \equiv \tilde{\alpha}_2/\tilde{\alpha}_1 = \alpha_2/\alpha_1$, $\Omega \equiv \frac{1}{2}g_{\rm eff}\mu_B B/E_0$, and $\kappa \equiv \tilde{\beta}/E_0$ or $\kappa \equiv \Delta/E_0$ depending on the origin of TE-TM splitting. The number of particles is given by $N = 2\pi\rho E_0/\tilde{\alpha}_1$, where $\rho \equiv \frac{1}{2\pi}\int_0^{2\pi}(|\psi_+|^2 + |\psi_-|^2)d\varphi$. We use x for φ in the main text to simplify the notation.

The early experimental and theoretical attempts [42–50] to estimate α_1 and α_2 generally agree that $\alpha_1 > 0$ and $\alpha_1 \gg |\alpha_2|$ with some works suggesting negative α_2. The recent investigations [51,52] of the ratio α_2/α_1 have shown that the ratio depends significantly on the detuning δ between exciton and photon modes and may change from very negative (smaller than -1 for small negative δ) to positive values (for larger δ). In our calculations throughout this paper, we use a "conservative" estimate $\alpha = -0.05$.

APPENDIX B: STABILITY ANALYSIS: NUMERICAL CALCULATIONS

We analyze the stability of the constant-amplitude solutions against the Bogoliubov-de Gennes excitations, see, e.g., Ref. [35]. Consider a small time-dependent perturbation $\varepsilon_\pm(x,t)$ around a stationary constant-amplitude solution,

$$\phi_\pm(x,t) = [\chi_\pm + \varepsilon_\pm(x,t)]e^{inx}. \tag{B1}$$

Substituting into (36) we get a system of linear equations on $\varepsilon_\pm(x,t)$,

$$\begin{aligned} i\dot{\varepsilon} &= -\varepsilon_\pm'' - 2i(n \mp 1)\varepsilon_\pm' + \chi_\pm^2(\varepsilon_\pm + \varepsilon_\pm^*) \\ &\quad + \alpha\chi_\pm\chi_\mp(\varepsilon_\mp + \varepsilon_\mp^*) + [-\mu + n^2 + \chi_\pm^2 \\ &\quad + \alpha\chi_\mp^2 \pm (\Omega - 2n)]\varepsilon_\pm + \kappa\varepsilon_\mp = 0. \end{aligned} \tag{B2}$$

Expanding $\varepsilon_\pm(x,t)$ into the Fourier series in x,

$$\varepsilon_\pm(x,t) = \sum_{l=-\infty}^{\infty} U_{\pm,l}(t)e^{ilx} + V_{\pm,l}^*(t)e^{-ilx}, \tag{B3}$$

we get a series of decoupled systems of equations parametrized by an integer l. To analyze the stability, we solve the eigenvalue problem

$$\hat{\eta}\mathcal{H}\mathbf{W} = \lambda\mathbf{W} \tag{B4}$$

with $\mathbf{W} = (U_{+,l}, V_{+,l}, U_{-,l}, V_{-,l})$,

$$\hat{\eta} = \begin{pmatrix} 1 & 0 & 0 & 0 \\ 0 & -1 & 0 & 0 \\ 0 & 0 & 1 & 0 \\ 0 & 0 & 0 & -1 \end{pmatrix} \tag{B5}$$

and

$$\mathcal{H} = \begin{pmatrix} d_+ & \chi_+^2 & \alpha\chi_+\chi_- + \kappa & \alpha\chi_+\chi_- \\ \chi_+^2 & \tilde{d}_+ & \alpha\chi_+\chi_- & \alpha\chi_+\chi_- + \kappa \\ \alpha\chi_+\chi_- + \kappa & \alpha\chi_+\chi_- & d_- & \chi_-^2 \\ \alpha\chi_+\chi_- & \alpha\chi_+\chi_- + \kappa & \chi_-^2 & \tilde{d}_- \end{pmatrix}, \tag{B6}$$

where $A_\pm$ and $B_\pm$ are given by

$$d_\pm \equiv l^2 + 2l(n \mp 1) + \chi_\pm^2 + [-\mu + m^2 + \chi_\pm^2 + \alpha\chi_\mp^2 \pm (\Omega - 2n)], \tag{B7}$$

$$\tilde{d}_\pm \equiv l^2 - 2l(n \mp 1) + \chi_\pm^2 + [-\mu + m^2 + \chi_\pm^2 + \alpha\chi_\mp^2 \pm (\Omega - 2n)]. \tag{B8}$$

The solution is spectrally unstable if there is at least one eigenvalue with a positive imaginary part $\mathrm{Im}\,\lambda > 0$.

APPENDIX C: STABILITY ANALYSIS: THEORY

Consider a small time-dependent perturbation $\varepsilon_\pm(x,t)$ around a stationary (in general, x-dependent) solution $\phi_\pm(x)$. For $\boldsymbol{\varepsilon} = (\varepsilon_+, \varepsilon_+^*, \varepsilon_-, \varepsilon_-^*)^T$, we get the equation

$$i\dot{\boldsymbol{\varepsilon}} = \hat{L}\boldsymbol{\varepsilon}, \tag{C1}$$

where $\hat{L} = \hat{\eta}\hat{H}$ with $\hat{\eta}$ defined above and

$$\hat{H} = \begin{pmatrix} \hat{D}_+ + 2|\phi_+|^2 + \alpha|\phi_-|^2 & \phi_+\phi_+ & \alpha\phi_-^*\phi_+ + \kappa & \alpha\phi_-\phi_+ \\ \phi_+^*\phi_+^* & \hat{D}_+^* + 2|\phi_+|^2 + \alpha|\phi_-|^2 & \alpha\phi_-^*\phi_+^* & \alpha\phi_-\phi_+^* + \kappa \\ \alpha\phi_+^*\phi_- + \kappa & \alpha\phi_+\phi_- & \hat{D}_- + 2|\phi_-|^2 + \alpha|\phi_+|^2 & \phi_-\phi_- \\ \alpha\phi_+^*\phi_-^* & \alpha\phi_+\phi_-^* + \kappa & \phi_-^*\phi_-^* & \hat{D}_-^* + 2|\phi_-|^2 + \alpha|\phi_+|^2 \end{pmatrix}. \tag{C2}$$

Substituting $\boldsymbol{\varepsilon}(x,t) = \boldsymbol{\varepsilon}(x)e^{-i\lambda t}$ to (C1), we get

$$\hat{L}\boldsymbol{\varepsilon} = \lambda\boldsymbol{\varepsilon}. \tag{C3}$$

Operator $\hat{L}$ has the following properties:

$$\hat{L}\boldsymbol{q}_1 = 0, \quad \hat{L}\boldsymbol{q}_2 = \boldsymbol{q}_1, \quad \hat{L}\hat{L}\boldsymbol{q}_2 = 0, \tag{C4}$$

where

$$\boldsymbol{q}_1 = \begin{pmatrix} \phi_+ \\ -\phi_+^* \\ \phi_- \\ -\phi_-^* \end{pmatrix}, \quad \boldsymbol{q}_2 = \frac{\partial}{\partial\mu}\begin{pmatrix} \phi_+ \\ \phi_+^* \\ \phi_- \\ \phi_-^* \end{pmatrix} \tag{C5}$$

are two zero modes of operator $\hat{L}^2$. Let us define the operator $\hat{L}^\dagger = \hat{H}\hat{\eta}$ conjugated to L with respect to the dot product

$$\langle \boldsymbol{f}, \boldsymbol{g} \rangle \equiv \int_0^{2\pi} \boldsymbol{f}^*(x) \cdot \boldsymbol{g}(x)\, dx. \tag{C6}$$

For $\hat{L}^\dagger$, we have

$$\hat{L}^\dagger\boldsymbol{Q}_1 = 0, \quad \hat{L}^\dagger\boldsymbol{Q}_2 = \boldsymbol{Q}_1, \quad \hat{L}^\dagger\hat{L}^\dagger\boldsymbol{Q}_2 = 0, \tag{C7}$$

where $\boldsymbol{Q}_{1,2} = \hat{\eta}\,\boldsymbol{q}_{1,2}$.

Suppose $\phi_\pm$ are calculated at $\kappa = 0$. Then there exists p_1 as well,

$$\hat{L}_0\boldsymbol{p}_1 = 0, \quad \hat{L}_0\boldsymbol{p}_2 = \boldsymbol{p}_1, \quad \hat{L}_0\hat{L}_0\boldsymbol{p}_2 = 0, \tag{C8}$$

where $\boldsymbol{p}_1$ and $\boldsymbol{p}_2$ are given by

$$\boldsymbol{p}_1 = \begin{pmatrix} -\phi_+ \\ \phi_+^* \\ \phi_- \\ -\phi_-^* \end{pmatrix}, \quad \boldsymbol{p}_2 = \frac{\partial}{\partial\Omega}\begin{pmatrix} \phi_+ \\ \phi_+^* \\ \phi_- \\ \phi_-^* \end{pmatrix}, \tag{C9}$$

and

$$\hat{L}_0^\dagger\boldsymbol{P}_1 = 0, \quad \hat{L}_0^\dagger\boldsymbol{P}_2 = \boldsymbol{P}_1, \quad \hat{L}_0^\dagger\hat{L}_0^\dagger\boldsymbol{P}_2 = 0 \tag{C10}$$

with $\boldsymbol{P}_{1,2} = \hat{\eta}\,\boldsymbol{p}_{1,2}$.

In the case when the state is split into two branches at $\kappa \neq 0$, we use a perturbative expansion for λ, a square root of the series in κ for an eigenvalue of operator $\hat{L}^2$,

$$\hat{L} = \hat{L}_0 + \kappa\hat{L}_1 + O(\kappa^2), \tag{C11}$$

$$\lambda = \kappa^{1/2}[\lambda_0 + \lambda_1\kappa + O(\kappa^2)], \tag{C12}$$

$$\boldsymbol{\varepsilon} = \boldsymbol{\varepsilon}_0 + \kappa^{1/2}\boldsymbol{\varepsilon}_1 + \kappa\boldsymbol{\varepsilon}_2 + O(\kappa^{3/2}). \tag{C13}$$

In the first orders, we have

$$\hat{L}_0\boldsymbol{\varepsilon}_0 = 0, \tag{C14}$$

$$\hat{L}_0\boldsymbol{\varepsilon}_1 = \lambda_0\boldsymbol{\varepsilon}_0, \tag{C15}$$

$$\hat{L}_0\boldsymbol{\varepsilon}_2 + \hat{L}_1\boldsymbol{\varepsilon}_0 = \lambda_0\boldsymbol{\varepsilon}_1. \tag{C16}$$

On applying L_0 from the left to the last equation,

$$\hat{L}_0^2\boldsymbol{\varepsilon}_2 + \hat{L}_0\hat{L}_1\boldsymbol{\varepsilon}_0 = \lambda_0^2\boldsymbol{\varepsilon}_0, \tag{C17}$$

and forming a dot product with $\boldsymbol{P}_2$, $\boldsymbol{Q}_2$,

$$\begin{aligned}\left\langle \boldsymbol{P}_2,\hat{L}_0^2\boldsymbol{\varepsilon}_2\right\rangle + \langle \boldsymbol{P}_2,\hat{L}_0\hat{L}_1\boldsymbol{\varepsilon}_0\rangle &= \lambda_0^2\langle \boldsymbol{P}_2,\boldsymbol{\varepsilon}_0\rangle\\ \left\langle \boldsymbol{Q}_2,\hat{L}_0^2\boldsymbol{\varepsilon}_2\right\rangle + \langle \boldsymbol{Q}_2,\hat{L}_0\hat{L}_1\boldsymbol{\varepsilon}_0\rangle &= \lambda_0^2\langle \boldsymbol{Q}_2,\boldsymbol{\varepsilon}_0\rangle\,, \end{aligned} \tag{C18}$$

$$\begin{aligned}\langle \boldsymbol{P}_1,\hat{L}_1\boldsymbol{\varepsilon}_0\rangle &= \lambda_0^2\langle \boldsymbol{P}_2,\boldsymbol{\varepsilon}_0\rangle\\ \langle \boldsymbol{Q}_1,\hat{L}_1\boldsymbol{\varepsilon}_0\rangle &= \lambda_0^2\langle \boldsymbol{Q}_2,\boldsymbol{\varepsilon}_0\rangle\,. \end{aligned} \tag{C19}$$

Due to the degeneracy, we take the linear superposition

$$\boldsymbol{\varepsilon}_0 = a\boldsymbol{p}_1 + b\boldsymbol{q}_1 \tag{C20}$$

with constant coefficients a and b, Thus

$$\begin{aligned} &a\langle \boldsymbol{P}_1,\hat{L}_1\boldsymbol{p}_1\rangle + b\langle \boldsymbol{P}_1,\hat{L}_1\boldsymbol{q}_1\rangle\\ &\quad -\lambda_0^2[a\langle \boldsymbol{P}_2,\boldsymbol{p}_1\rangle + b\langle \boldsymbol{P}_2,\boldsymbol{q}_1\rangle] = 0\\ &a\langle \boldsymbol{Q}_1,\hat{L}_1\boldsymbol{p}_1\rangle + b\langle \boldsymbol{Q}_1,\hat{L}_1\boldsymbol{q}_1\rangle\\ &\quad -\lambda_0^2[a\langle \boldsymbol{Q}_2,\boldsymbol{p}_1\rangle + b\langle \boldsymbol{Q}_2,\boldsymbol{q}_1\rangle] = 0. \end{aligned} \tag{C21}$$

Also, as $\hat{L}(\kappa)\boldsymbol{q}_1(\kappa) = 0$ for arbitrary κ, there exist $\tilde{\boldsymbol{q}}_1$ and $\tilde{\boldsymbol{Q}}_1$ such that $\hat{L}_1\boldsymbol{q}_1 = \hat{L}_0\tilde{\boldsymbol{q}}_1$ and $\hat{L}_1^\dagger\boldsymbol{Q}_1 = \hat{L}_0^\dagger\tilde{\boldsymbol{Q}}_1$. Therefore $\langle \boldsymbol{P}_1,\hat{L}_1\boldsymbol{q}_1\rangle = \langle \boldsymbol{Q}_1,\hat{L}_0\tilde{\boldsymbol{q}}_1\rangle = 0$, $\langle \boldsymbol{Q}_1,\hat{L}_1\boldsymbol{q}_1\rangle = \langle \boldsymbol{Q}_1,\hat{L}_0\tilde{\boldsymbol{q}}_1\rangle = 0$, and $\langle \boldsymbol{Q}_1,\hat{L}_1\boldsymbol{p}_1\rangle = \langle \tilde{\boldsymbol{Q}}_1,\hat{L}_0\boldsymbol{p}_1\rangle = 0$:

$$\begin{aligned} a\big(\langle \boldsymbol{P}_1,\hat{L}_1\boldsymbol{p}_1\rangle - \lambda_0^2\langle \boldsymbol{P}_2,\boldsymbol{p}_1\rangle\big) - \lambda_0^2 b\langle \boldsymbol{P}_2,\boldsymbol{q}_1\rangle &= 0\\ a\lambda_0^2\langle \boldsymbol{Q}_2,\boldsymbol{p}_1\rangle + \lambda_0^2 b\langle \boldsymbol{Q}_2,\boldsymbol{q}_1\rangle &= 0. \end{aligned} \tag{C22}$$

Thus, for the two nonzero eigenvalues λ_0, we have the equation

$$\lambda_0^2 = \frac{\langle \boldsymbol{P}_1,\hat{L}_1\boldsymbol{p}_1\rangle\langle \boldsymbol{Q}_2,\boldsymbol{q}_1\rangle}{\langle \boldsymbol{Q}_2,\boldsymbol{q}_1\rangle\langle \boldsymbol{P}_2,\boldsymbol{p}_1\rangle - \langle \boldsymbol{Q}_2,\boldsymbol{p}_1\rangle\langle \boldsymbol{P}_2,\boldsymbol{q}_1\rangle}. \tag{C23}$$

Evaluating $\boldsymbol{p}_1,\boldsymbol{q}_1$, $\boldsymbol{P}_2,\boldsymbol{Q}_2$ for the TSM state $\Delta m = 2$ at $\kappa = 0$ [see Eqs. (10), (13), and (14)] we get $\langle \boldsymbol{Q}_2,\boldsymbol{p}_1\rangle = 0$, $\langle \boldsymbol{P}_2,\boldsymbol{q}_1\rangle = 0$, $\langle \boldsymbol{P}_2,\boldsymbol{p}_1\rangle = 4\pi/(1-\alpha)$, $\langle \boldsymbol{Q}_2,\boldsymbol{q}_1\rangle = 4\pi/(1+\alpha)$. Therefore, for λ_0^2, we have

$$\lambda_0^2 = \frac{\langle \boldsymbol{P}_1,\hat{L}_1\boldsymbol{p}_1\rangle}{\langle \boldsymbol{P}_2,\boldsymbol{p}_1\rangle} = \frac{(1-\alpha)}{4\pi}\langle \boldsymbol{p}_1,\hat{H}_1\boldsymbol{p}_1\rangle\,. \tag{C24}$$

Operator H_1 can be found by substituting the perturbative solution for the TSM state into (C2). Evaluating (C24), we get the formula (45).

From the system (C22), we find coefficients a and b, which define the instability mode (C20). For the considered case, we get $b = 0$ and therefore the unstable mode is $\varepsilon_\pm \sim \pm\chi_\pm e^{inx}$.

[1] H. Deng, H. Haug, and Y. Yamamoto, Rev. Mod. Phys. **82**, 1489 (2010).
[2] I. Carusotto and C. Ciuti, Rev. Mod. Phys **85**, 299 (2013).
[3] A. Amo *et al.*, Nature (London) **457**, 291 (2009).
[4] K. G. Lagoudakis, M. Wouters, M. Richard, A. Baas, I. Carusotto, R. André, Le Si Dang, and B. Deveaud-Plédran, Nat. Phys. **4**, 706 (2008).
[5] K. G. Lagoudakis, T. Ostatnický, A. V. Kavokin, Y. G. Rubo, R. André, and B. Deveaud-Plédran, Science **326**, 974 (2009).
[6] M. Sich, D. N. Krizhanovskii, M. S. Skolnick, A. V. Gorbach, R. Hartley, D. V. Skryabin, E. A. Cerda-Méndez, K. Biermann, R. Hey, and P. V. Santos, Nat. Photon. **6**, 50 (2011).
[7] M. Abbarchi, A. Amo, V. G. Sala, D. D. Solnyshkov, H. Flayac, L. Ferrier, I. Sagnes, E. Galopin, A. Lemaitre, G. Malpuech, and J. Bloch, Nat. Phys. **9**, 275 (2013).
[8] C. Leyder, M. Romanelli, J. Ph. Karr, E. Giacobino, T. C. H. Liew, M. M. Glazov, A. V. Kavokin, G. Malpuech, and A. Bramati, Nat. Phys. **3**, 628 (2007).
[9] I. A. Shelykh, A. V. Kavokin, Yuri G. Rubo, T. C. H. Liew, and G. Malpuech, Semicond. Sci. Technol. **25**, 013001 (2010).
[10] D. Ballarini, M. De Giorgi, E. Cancellieri, R. Houdré, E. Giacobino, R. Cingolani, A. Bramati, G. Gigli, and D. Sanvitto, Nat. Commun. **4**, 1778 (2013).
[11] C. Sturm *et al.*, Nat. Commun. **5**, 3278 (2014).
[12] S. Christopoulos, G. Baldassarri Hoger von Hogersthal, A. Grundy, P. G. Lagoudakis, A. V. Kavokin, J. J. Baumberg, G. Christmann, R. Butte, E. Feltin, J. F. Carlin, and N. Grandjean, Phys. Rev. Lett. **98**, 126405 (2007)
[13] C. Schneider *et al.*, Nature (London) **497**, 348 (2013).
[14] V. P. Kochereshko *et al.*, Sci. Rep. **6**, 20091 (2016).
[15] D. D. Solnyshkov, M. M. Glazov, I. A. Shelykh, A. V. Kavokin, E. L. Ivchenko, and G. Malpuech, Phys. Rev. B **78**, 165323 (2008)
[16] B. Pietka, D. Zygmunt, M. Krol, M. R. Molas, A. A. L. Nicolet, F. Morier-Genoud, J. Szczytko, J. Lusakowski, P. Zieba, I. Tralle, P. Stepnicki, M. Matuszewski, M. Potemski, and B. Deveaud, Phys. Rev. B **91**, 075309 (2015).
[17] Yuri G. Rubo, A. V. Kavokin, and I. A. Shelykh, Phys. Lett. A **358**, 227 (2006).
[18] A. V. Larionov, V. D. Kulakovskii, S. Höfling, C. Schneider, L. Worschech, and A. Forchel, Phys. Rev. Lett. **105**, 256401 (2010).
[19] C. Sturm, D. Solnyshkov, O. Krebs, A. Lemaître, I. Sagnes, E. Galopin, A. Amo, G. Malpuech, and J. Bloch, Phys. Rev. B **91**, 155130 (2015).
[20] P. Walker, T. C. H. Liew, D. Sarkar, M. Durska, A. P. D. Love, M. S. Skolnick, J. S. Roberts, I. A. Shelykh, A. V. Kavokin, and D. N. Krizhanovskii, Phys. Rev. Lett. **106**, 257401 (2011).
[21] J. Fischer, S. Brodbeck, A. V. Chernenko, I. Lederer, A. Rahimi-Iman, M. Amthor, V. D. Kulakovskii, L. Worschech, M. Kamp, M. Durnev, C. Schneider, A. V. Kavokin, and S. Hofling, Phys. Rev. Lett. **112**, 093902 (2014).
[22] I. A. Shelykh, Yu. G. Rubo, and A. V. Kavokin, Superlattices Microstruct. **41**, 313 (2007).
[23] I. A. Shelykh, G. Pavlovic, D. D. Solnyshkov, and G. Malpuech, Phys. Rev. Lett. **102**, 046407 (2009).
[24] G. Liu, D. W. Snoke, A. Daley, L. N. Pfeiffer, and K. West, Proc. Natl. Acad. Sci. **112**, 2676 (2015).
[25] V. G. Sala *et al.*, Phys. Rev. X **5**, 011034 (2015).
[26] Y. G. Rubo, Phys. Rev. Lett. **99**, 106401 (2007).

[27] H. Flayac, I. A. Shelykh, D. D. Solnyshkov, and G. Malpuech, Phys. Rev. B **81**, 045318 (2010).
[28] M. Toledo Solano and Yuri G. Rubo, Phys. Rev. B **82**, 127301 (2010).
[29] H. Flayac, D. D. Solnyshkov, G. Malpuech, and I. A. Shelykh, Phys. Rev. B **82**, 127302 (2010).
[30] M. Toledo-Solano, M. E. Mora-Ramos, A. Figueroa, and Y. G. Rubo, Phys. Rev. B **89**, 035308 (2014).
[31] A. Kuther, M. Bayer, T. Gutbrod, A. Forchel, P. A. Knipp, T. L. Reinecke, and R. Werner, Phys. Rev. B **58**, 15744 (1998).
[32] A. V. Kavokin, J. J. Baumberg, G. Malpuech, and F. P. Laussy, *Microcavities* (Oxford University Press, Oxford, 2007).
[33] L. D. Carr, Charles W. Clark, and W. P. Reinhardt, Phys. Rev. A **62**, 063610 (2000).
[34] The term "topological spin Meissner effect" introduced here should not be confused with the "topological Meissner effect" used to describe a strongly anisotropic Meissner effect originating from chiral d-density waves studied in. P. Kotetes and G. Varelogiannis, Phys. Rev. B **78**, 220509 (2008).
[35] D. V. Skryabin, Phys. Rev. A **63**, 013602 (2000).
[36] M. M. Sternheim and J. F. Walker, Phys. Rev. C **6**, 114 (1972).
[37] See Supplemental Material at http://link.aps.org/supplemental/10.1103/PhysRevB.94.115407 for more details on the dynamics of instability modes, approximate solutions for constant-amplitude topological spin Meissner states in the presence of TE-TM splitting, stability analysis of constant amplitude solutions with respect to individual angular harmonics, comparison between theoretically and numerically found symmetry-breaking solutions, and video of animated dynamics of instabilities.
[38] G. Dasbach, C. Diederichs, J. Tignon, C. Ciuti, Ph. Roussignol, C. Delalande, M. Bayer, and A. Forchel, Phys. Rev. B **71**, 161308(R) (2005).
[39] S. Dufferwiel, F. Li, E. Cancellieri, L. Giriunas, A. A. P. Trichet, D. M. Whittaker, P. M. Walker, F. Fras, E. Clarke, J. M. Smith, M. S. Skolnick, and D. N. Krizhanovskii, Phys. Rev. Lett. **115**, 246401 (2015).
[40] G. Panzarini, L. C. Andreani, A. Armitage, D. Baxter, M. S. Skolnick, V. N. Astratov, J. S. Roberts, A. V. Kavokin, M. R. Vladimirova, and M. A. Kaliteevski, Phys. Rev. B **59**, 5082 (1999).
[41] M. Z. Maialle, E. A. de Andrada e Silva, and L. J. Sham, Phys. Rev. B **47**, 15776 (1993).
[42] P. Renucci, T. Amand, X. Marie, P. Senellart, J. Bloch, B. Sermage, and K. V. Kavokin, Phys. Rev. B **72**, 075317 (2005).
[43] J. Kasprzak, R. André, Le Si Dang, I. A. Shelykh, A. V. Kavokin, Yuri G. Rubo, K. V. Kavokin, and G. Malpuech, Phys. Rev. B **75**, 045326 (2007).
[44] M. Vladimirova, S. Cronenberger, D. Scalbert, M. Nawrocki, A. V. Kavokin, A. Miard, A. Lemaître, and J. Bloch, Phys. Rev. B **79**, 115325 (2009).
[45] Z. Vörös, D. W. Snoke, L. Pfeiffer, and K. West, Phys. Rev. Lett. **103**, 016403 (2009).
[46] F. Tassone and Y. Yamamoto, Phys. Rev. B **59**, 10830 (1999).
[47] M. Combescot, O. Betbeder-Matibet, and R. Combescot, Phys. Rev. Lett. **99**, 176403 (2007).
[48] S. Schumacher, N. H. Kwong, and R. Binder, Phys. Rev. B **76**, 245324 (2007).
[49] M. M. Glazov, H. Ouerdane, L. Pilozzi, G. Malpuech, A. V. Kavokin, and A. D'Andrea, Phys. Rev. B **80**, 155306 (2009).
[50] M. Wouters, Phys. Rev. B **76**, 045319 (2007).
[51] M. Vladimirova, S. Cronenberger, D. Scalbert, K. V. Kavokin, A. Miard, A. Lemaître, J. Bloch, D. Solnyshkov, G. Malpuech, and A. V. Kavokin, Phys. Rev. B **82**, 075301 (2010).
[52] N. Takemura, S. Trebaol, M. Wouters, M. T. Portella-Oberli, and B. Deveaud, Phys. Rev. B **90**, 195307 (2014).